Astronomy & Astrophysics manuscript no. cocor6 February 5, 2008
(DOI: will be inserted by hand later)

Fundamental parameters of Be stars located in the seismology fields of COROT ⋆

Y. Frémat[1], C. Neiner[2,3], A.-M. Hubert[3], M. Floquet[3], J. Zorec[4], E. Janot-Pacheco[5], and J. Renan de Medeiros[6]

[1] Royal Observatory of Belgium, 3 avenue circulaire, 1180 Brussels, Belgium
[2] Institute for astronomy, KU Leuven, Celestijnenlaan 200B, 3001 Leuven, Belgium
[3] GEPI / UMR 8111 du CNRS, Observatoire de Paris-Meudon, 5 place Jules Janssen, 92195 Meudon, France
[4] Institut d'Astrophysique de Paris, UMR 7095 CNRS, Université Pierre & Marie Curie
[5] Instituto de Astronomia, Geofísica e Ciências Atmosféricas, Universidade de São Paulo, Rua do Matão 1226, 05508-090 São Paulo, Brazil
[6] Departamento de Fisica, Universidade Federal do Rio Grande do Norte, 59072-970 Natal, Brazil

Accepted date: October 27, 2005

Abstract. In preparation for the COROT space mission, we determined the fundamental parameters (spectral type, temperature, gravity, $V \sin i$) of the Be stars observable by COROT in its seismology fields (64 Be stars). We applied a careful and detailed modeling of the stellar spectra, taking into account the veiling caused by the envelope, as well as the gravitational darkening and stellar flattening due to rapid rotation. Evolutionary tracks for fast rotators were used to derive stellar masses and ages. The derived parameters will be used to select Be stars as secondary targets (i.e. observed for 5 consecutive months) and short-run targets of the COROT mission. Furthermore, we note that the main part of our stellar sample is falling in the second half of the main sequence life time, and that in most cases the luminosity class of Be stars is inaccurate in characterizing their evolutionary status..

Key words. Stars: emission-line, Be – Stars: activity – Stars: fundamental parameters – Stars: statistics

1. Introduction

1.1. Be stars

Be stars are non-supergiant B stars that show or have shown at one or another moment Hα emission (Jaschek et al. 1981). More generally, emission does not only occur in the first members of the Balmer line series, but can also affect the continuum and line profiles of other atoms or ions, such as Fe . It is generally agreed that, in classical Be stars, this emission is due to the presence of a cool, disk-like circumstellar envelope concentrated in the equatorial plane. For a complete review of the "Be phenomenon" and its characteristics, see Porter & Rivinius (2003).

Classical Be stars are fast rotators. Statistical studies indeed suggest that their angular speed ranges from 60 to 100% of the critical breakup velocity (Ω_c), with a narrow maximum occurrence at 80% (Chauville et al. 2001) or at 90% when accounting for fast rotation effects (Frémat et al. 2005) in order to limit the saturation of the lines' FWHM at high rotation rates (Townsend et al. 2004).

Although we know that the envelopes of classical Be stars are probably formed during episodes of strong mass ejection, the precise origin of these ejections is still unknown and may differ from star to star. One of the currently most interesting explanations resides in the fast (non-critical) rotation and the beating of non-radial pulsation (NRP) modes combining their effects to cause matter expulsion. In the H-R diagram, early Be stars are indeed located at the lower border of the instability strip of the β Cep stars, while mid and late Be stars are mixed with Slowly Pulsating B (SPB) stars. Short and long period pulsations are therefore expected and confirmed in the majority of Be stars, if we except the late sub-classes. From the Hipparcos database (Hubert & Floquet 1998) it was shown that short-term variability is present in almost all early-Be stars (86%), while it seems to be less common in the cooler ones (40% to 18% from the mid to the latest spectral types). This fact, however, could be due to the variability detection level of current in-

Send offprint requests to: Y. Frémat, e-mail: yves.fremat@oma.be

⋆ Based on GAUDI, the data archive and access system of the ground-based asteroseismology programme of the COROT mission. The GAUDI system is maintained at LAEFF (http://ines.laeff.esa.es/corot/). LAEFF is part of the Space Science Division of INTA. Also based on OHP (Observatoire de Haute-Provence, France), LNA (Laboratório Nacional de Astrofísica, Brazil) and FEROS (ESO, 072.D-0315(A)) observations. A part of the Tables and Figures described in this paper are available at the CDS (Centre de Données astronomiques de Strasbourg: http://cdsweb.u-strasbg.fr/cats/cats.html).

strumentation, since the amplitude of pulsations in late subtypes of B stars is expected to be very small (a few mmag). Up to now, about hundred Be stars have already been claimed as short-term periodic variables (hours, tens of hours) and their number is still increasing. However, the detection of short and long-term pulsations is difficult using ground-based observations even in the framework of multisite campaigns (e.g. the Musicos 98 campaign, see Neiner et al. 2002). The prediction and the study of the coincidence between the beating of multiperiodic pulsations and the occurrence of mass-ejection further needs the determination of accurate periods and the detection of the most complete sample of pulsation modes, which is not an easy matter, even during multisite campaigns. Although multiperiodicity has been detected in several Be stars (e.g. 66 Oph, Floquet et al. 2002), only one such coincidence case between beating and matter ejection has been reported until now (μ Cen, Rivinius et al. 1998). As a matter of fact, most of the presently known cases of pulsation in Be stars result from high-resolution spectroscopy. This technique is very powerful in identifying high-order pulsation modes, but not well adapted to resolve closely spaced multiple periods. Photometry with COROT will therefore provide a much more superior observing tool to detect new multiperiodic pulsators among Be stars.

In this framework, the COROT mission will provide us with 5-months continuous observations of a substantial amount of Be stars. It will allow us to reach a never achieved precision in the determination of pulsation frequencies, further giving us the opportunity to study their possible magnetic splitting and the rotational modulation in Be stars.

1.2. The COROT mission

The COROT (COnvection, ROtation and planetary Transits) satellite[1] will be launched in August 2006 and has two goals: to study the interior of stars by looking at their oscillations and to search for extrasolar planets by detecting planetary transits (see Baglin et al. 2002). Therefore four CCDs are used: two for the asteroseismology program and two for the exoplanetary program. The asteroseismology CCDs are positioned on the sky to observe simultaneously one (or sometimes two) bright (V $\sim$ 5.5) primary target(s) plus eight or nine surrounding secondary targets with a magnitude $5.6 \leq V \leq 9.4$.

The 30 cm telescope of COROT will be pointed alternatively towards the galactic centre and anticentre. These two cones of observations, which have a radius of 10 degrees, are the pointing limits for the CCDs. The two asteroseismology CCDs cover a field of view of 1.3×2.6 degrees. At least 5 such fields will be observed by COROT during $\sim$5 months each. Finally, short observing runs (20-30 days) will be performed on specific targets so that the full target list covers as well as possible the HR diagram.

Bright Be stars can therefore be observed either as secondary targets of the asteroseismology program in long runs, or as short runs targets. An international collaboration led by A.-M. Hubert is preparing these observations. In this paper, we present the procedure that was carried out to perform a preliminary analysis of as many bright ($5.6 < V < 9.4$) classical Be stars as possible in the observing cones of COROT. The position, spectral type and variability of these Be stars are factors taken into account for the selection of the fields that will be observed by COROT. To carry out this first target selection, we therefore need good stellar parameters with typical accuracies of 10 % on the effective temperature ($T_{\rm eff}$), of 0.1 to 0.2 dex on the surface gravity ($\log\ g$), and of 5 to 10 % on the projected rotation velocity ($V \sin i$). To be valuable, the parameters determination further needs to account for the peculiar nature of Be stars, including the effects of fast rotation, circumstellar emission, and departure from LTE.

Table 1. Sample of spectra used for this study. A complete version of the table is available at the CDS (http://cdsweb.u-strasbg.fr/cats/cats.html). For the ELODIE spectra, the signal to noise ratio (S/N) was provided by the INTERTACOS (OHP) reduction pipeline, while for the other data it was computed with IRAF by selecting some parts of the continuum in the studied spectral region. '[1]' indicates that the spectrum is available in GAUDI.

HD	Obs. date	$T_{\rm exp}$ (s)	Instrument	S/N
42406	2004-02-05	900	FEROS	249
43264	2001-11-27	3300	ELODIE[1]	83
43285	2001-12-21	1800	ELODIE[1]	123
44783	2000-12-18	1500	ELODIE[1]	121
45901	2004-01-03	2700	AURELIE 4280_G3	120
46380	2001-12-22	3600	ELODIE[1]	53
46484	2003-01-26	3600	ELODIE[1]	107
47054	2002-01-28	300	FEROS[1]	145
... A complete version of the table is available at the CDS				

Most of the data used in this study are available on the GAUDI (Ground-based Asteroseismology Uniform Database Interface) database (Solano et al. 2005) and are described in Sect 2. In GAUDI, more specific informations, such as fundamental stellar parameters (surface gravity and effective temperature) and projected rotation velocities, can also be found and were automatically derived from the observations. However, these parameters were obtained without accounting for neither circumstellar emission nor fast rotation effects, which are generally expected to affect the spectra of Be stars. The goal of the present work is therefore to reestimate the effective temperature ($T_{\rm eff}$), surface gravity ($\log\ g$) and projected rotation velocity ($V \sin i$) accounting, as far as possible, for the peculiar nature of Be stars, in order to update the GAUDI database and thus facilitate the target selection for COROT.

For the same reasons, this work also aims at identifying the stars in our sample that could be considered as *particular*, such as Herbig stars or spectroscopic binaries with a Be star component. The model atmospheres we used are defined in Sect. 3, while the procedure we adopted to perform these determinations is detailed in Sect. 4. Our results are listed in Sect. 5, with remarks concerning several specific targets gathered in Sect. 6, and discussed in Sect. 7.

[1] http://corot.oamp.fr/

2. Observations

In preparation for the COROT satellite observations, an ambitious ground-based observing program was performed (P.I.: C. Catala, Observatoire de Paris). For each star with a magnitude between 5.6 and 8 located in the observing cones of the COROT satellite, at least one spectrum was obtained and stored in the GAUDI database. The sample of stars we are studying in the present paper is therefore a sub-sample of the compilation by Solano et al. (2005). It gathers the targets that are well known Be stars or that were recently identified as Be stars (Neiner et al. 2005).

The data were mainly obtained with two high-resolution échelle spectrographs (R ∼ 40000 – 50000): ELODIE at the 2m telescope of the Observatoire de Haute-Provence (OHP, France) and FEROS at the 1.5m and 2.2m telescopes of ESO (La Silla, Chile). Additional observations were also obtained at the 1.9 meter telescope at SAAO (South Africa) with the GIRAFFE spectrograph, with the CORALIE spectrograph on 1.2 m Swiss telescope in La Silla (Chile), with the SARG (Spectrografo Alta Risoluzione Galileo) spectrograph at the 3.6m Telescopio Nazionale Galileo (TNG, La Palma, Spain) and with the Coudé spectrograph on the 2 meter telescope of the Tautenburg observatory (Germany).

To complete the sample of Be stars in the observing cones of COROT, additional spectra of Be stars with a magnitude between 8 and 9.4 were obtained: in Brazil, at the LNA (Laboratório Nacional de Astrofisica, Observatrio do Pico dos Dias) with the Cassegrain spectrograph (OPD CASS) attached to the 1.6 m Boller & Chivens telescope and using the 900 lines/mm grating (R ∼ 7000); in France, at the OHP (Observatoire de Haute-Provence) with AURELIE (1.52-m telescope) at medium resolution (R ∼ 15000 with the grating N^{o}2, $\Delta\lambda$ = 220 Å) and lower resolution (R ∼ 7000 with the grating N^{o}3, $\Delta\lambda$ = 440 Å); and in Chile with FEROS (ESO) on Brazilian time.

In principle, the sample of studied stars contains all Be stars in the observing cones of COROT with the adequate magnitude ($5.6 \leq V \leq 9.4$). The target list was compiled using SIMBAD and adding newly discovered Be stars from Neiner et al. (2005). However, known SB2 with a Be star component and interacting Be binaries were rejected from the list of possible Be targets. A few faint Be stars are also not studied in this paper because no spectra were obtained due to bad weather conditions. As a consequence, the sample of studied Be stars is not complete, but no systematic bias is expected. In particular, the samples in the centre and anticenter direction are equivalent.

3. Model atmospheres and flux grids

The plane-parallel atmosphere models we used for effective temperatures ranging from 15000 K to 27000 K were computed in two consecutive steps. To account in the most effective way for line-blanketing, the temperature structure of the atmospheres was computed by Kurucz (1993) using the ATLAS9 FORTRAN program. Non-LTE level populations were then calculated for each of the atoms we considered using (Hubeny & Lanz 1995) and keeping fixed the temperature and density distributions. The surface chemical abundances we adopted are those published by Grevesse & Sauval (1998) for the Sun.

Table 2 lists the ions we introduced in the computations. Except for C , the atomic models we used in this work were downloaded from 's homepage[2] maintained by I. Hubeny and T. Lanz. C was treated thanks to the IDL package developed by Varosi et al. (1995) and by adopting the atomic data (oscillator strengths, energy levels and photoionization cross sections) selected from the database (Cunto et al. 1993). It reproduces the results obtained by Sigut (1996).

Table 2. Atoms and ions treated in our computations assuming NLTE. The number of levels taken into account for each ion is also given.

Atom	Ion	Levels
Hydrogen	H	8 levels + 1 superlevel
	H	1 level
Helium	He	24 levels
	He	20 levels
	He	1 level
Carbon	C	53 levels all individual levels
	C	12 levels
	C	9 levels + 4 superlevels
	C	1 level
Nitrogen	N	13 levels
	N	35 levels + 14 superlevels
	N	11 levels
	N	1 level
Oxygen	O	14 levels + 8 superlevels
	O	36 levels + 12 superlevels
	O	9 levels
	O	1 level
Magnesium	Mg	21 levels + 4 superlevels
	Mg	1 level

Model atmospheres with effective temperatures lower than 15000 K were treated assuming full LTE, while those hotter than 27000 K were taken from the OSTAR2002 NLTE grid (Lanz & Hubeny 2003). The grid of fluxes we use during the fitting procedure (Sect. 4.1) was finally built with and for effective temperatures and surface gravities ranging from 8000 to 50000 K and from 2.5 to 4.5 dex (cgs) respectively.

4. Adopted procedure

To take into account the main phenomena expected to affect the spectra of Be stars, the determination of their fundamental parameters was carried out in three consecutive steps, each of them being described in the following sections and summarized in Fig. 2.

[2] http://tlusty.gsfc.nasa.gov

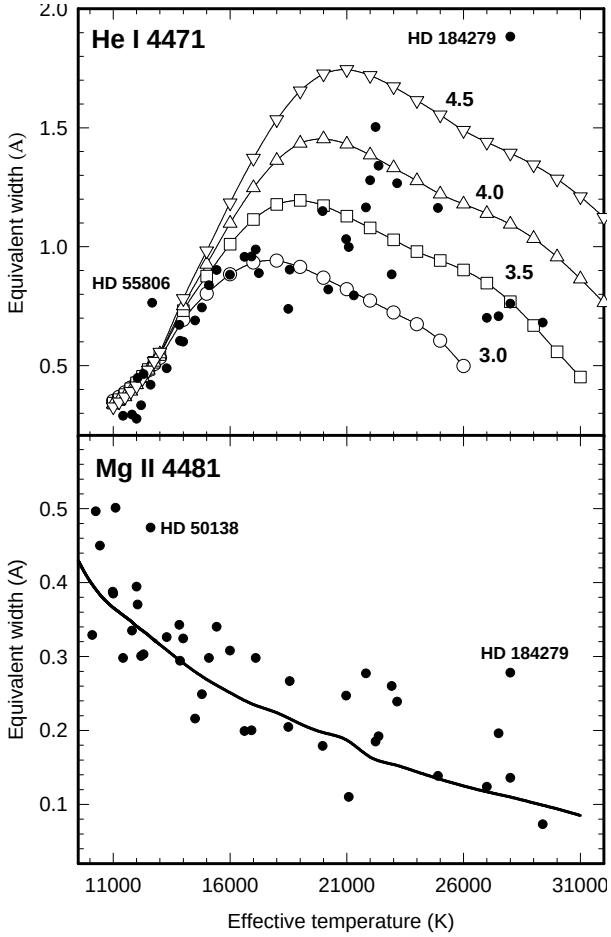

Fig. 1. Computed (curves) and observed (filled circles) equivalent widths for the He 4471 (upper panel) and Mg 4481 (lower panel) spectral lines are shown. The surface gravity adopted in the calculations is noted on each curve. Mg 4481 has a very weak luminosity-dependence, for clarity we therefore plotted only the theoretical line corresponding to log $g = 4.0$. Computations are made using plane-parallel model atmospheres (Sect. 3).

4.1. Apparent fundamental parameters determination

Hydrogen, helium and Mg lines are generally assumed to be good temperature and gravity indicators for the study of B-type stars. Fig. 1 shows the variation of the equivalent width computed for the He 4471 and Mg 4481 spectral lines with effective temperature and surface gravity. Their different broadening mechanisms and transition probabilities further present the advantage to have been studied with great detail for a long time, allowing accurate line profile computations. In our procedure, we therefore mainly focus on a spectral domain ranging from 4000 to 4500 Å (see line-identification and computed equivalent widths in Table 3), which gathers no less than two hydrogen lines, 5 strong helium lines and 2 blended Mg lines. Observations obtained in this region, and for each of the considered Be stars, are compared to a grid of synthetic spectra (see Steps 1 and 2 of Fig. 2). For efficiency reasons, this comparison is performed by means of a least squares method based on the minimization package developed at CERN,

Table 3. Theoretical equivalent widths of the main spectral lines found in the considered spectral region and for various spectral types. Computations are made using plane-parallel model atmospheres (Sect. 3). Effective temperatures and spectral types are taken from Gray & Corbally (1994).

Ion	λ (Å)	Equivalent width (mÅ)			
		B0V	B2V	B5V	B8V
		29000 K	19500 K	14000 K	11550 K
He	4009	334	613	217	48
He	4026	908	1541	878	542
H	4102	3869	6452	9358	11475
He	4121	450	251	82	32
He	4144	443	765	322	120
He	4169	88	91	32	5
C	4267	215	270	97	49
H	4340	3724	6368	9552	12032
He	4388	537	950	378	220
He	4471	1087	1442	667	345
Mg	4481	122	198	272	318

which we transposed to a FORTRAN computer code named , and which allows to deal with large datasets. interpolates the spectra in a grid of stellar fluxes computed with plane-parallel model atmospheres (see Sect. 3) for different values of the effective temperature and of the surface gravity. To account for the instrumental resolution and the Doppler broadening due to rotation, the spectra are then convolved with a Gaussian function using subroutines taken from the computer code provided with (Hubeny & Lanz 1995). During the fitting procedure, 5 free parameters are considered: the effective temperature $T_{\rm eff}$, the surface gravity $\log g$, the projected rotation velocity $V \sin i$, the radial velocity $V_{\rm rad}$ and the wavelength-independent ratio between the mean "flux" level of the normalized observed and theoretical spectra, i.e. a scaling factor allowing to match the stellar continuum. The χ^2 parameter is computed on different spectral zones chosen from 4000 to 4500 Å. These zones are selected in order to exclude any part of the spectrum that could be affected by line emission or shell absorption (e.g. hydrogen line cores) or/and by interstellar absorption bands (generally found between 4400 and 4450 Å). As the parameters derived in this way do not take into account the effects of stellar flattening and gravitational darkening due to fast rotation, they will be further called *apparent* fundamental parameters and correspond to what is obtained when assuming that the star is a sphere with uniform temperature and density surface distributions.

4.2. Veiling caused by the envelope

The spectra of Be stars are not only affected by line-emission, but they are also proportionally affected by continuum emission and electron scattering, which change the stellar continuum level. When significant, emission or/and scattering cause an artificial weakening of the spectral line intensity generally leading to underestimation of the effective temperature and of

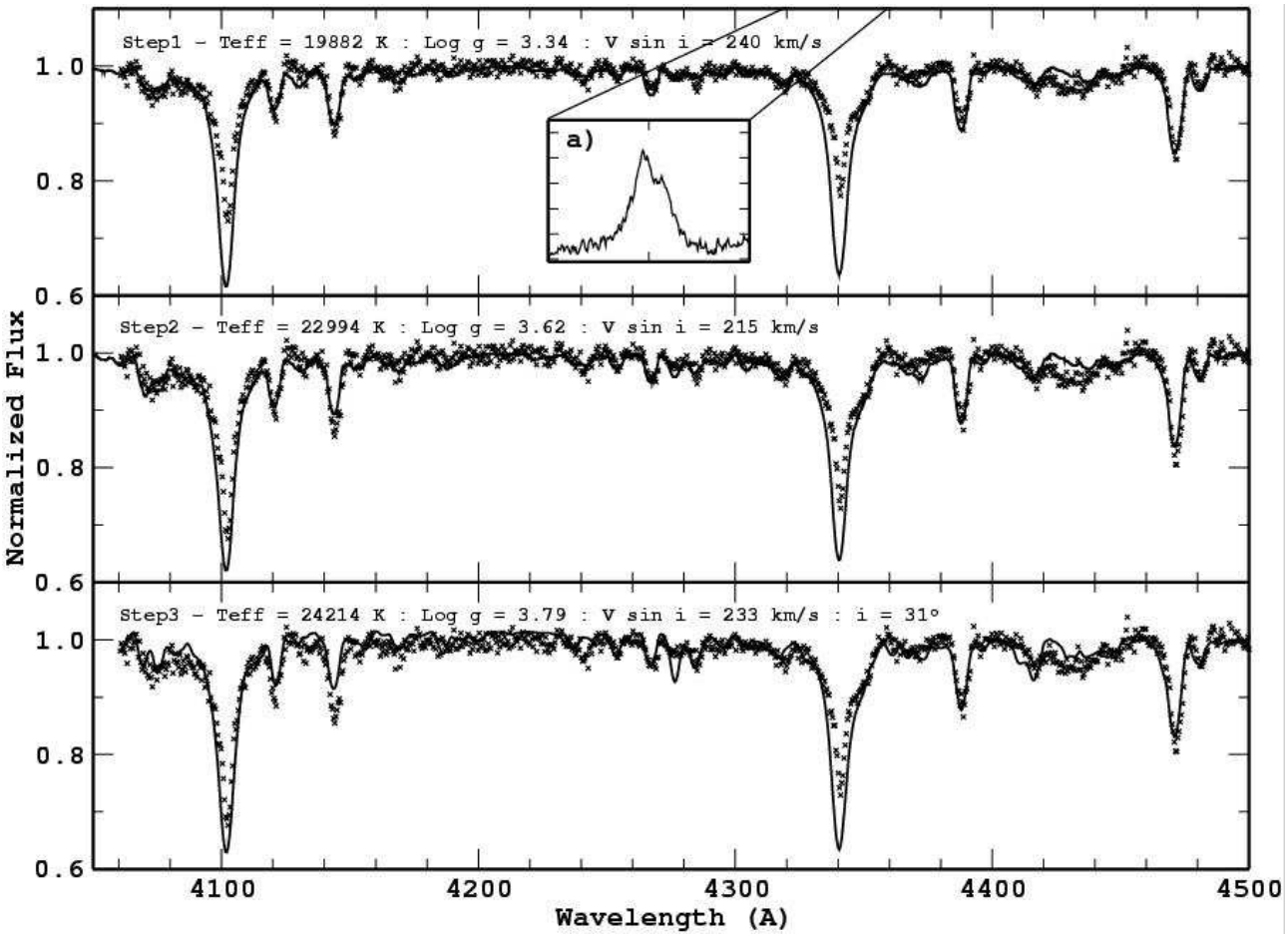

Fig. 2. Description of the three-steps procedure adopted to derive the fundamental parameters. **Step 1:** Fit of the observed spectrum (crosses) with synthetic spectra (solid line), ignoring continuum veiling and second order fast-rotation effects. Subtracting the observed Hγ line-profile from the synthetic one allows us to estimate the magnitude of the circumstellar emission (panel a). **Step 2:** Observations are corrected for veiling and fitted again. **Step 3:** The fundamental parameters derived in step 2 are corrected to account for fast rotation effects with a new fit at Ω/Ω_c=0.99.

the surface gravity in B-type stars. Ballereau et al. (1995) estimated the magnitude of this veiling by studying hydrogen and helium lines and proposed an empirical approach to correct the stellar spectra from its effects. They mainly introduce a correction term, r, which they found directly proportional to the intensity or to the equivalent width of the Hγ line-emission W_e(Hγ) (see Step 1 of Fig. 2).

To measure the magnitude of the Hγ emission, the synthetic Hγ profile obtained from a first fit of the fundamental parameters was subtracted from the observations (see Fig. 2). The result was wavelength-integrated in order to obtain W_e(Hγ), and to interpolate the r value from Fig. 9a in Ballereau et al. (1995). When greater than zero, this correction was directly applied to the observations (see Eq. 1 in Ballereau et al. 1995), which were finally used to re-derive the fundamental parameters (see Sect. 4.1).

4.3. Gravitational darkening and stellar flattening

As mentioned in the introduction, Be stars are fast rotators with angular velocities probably around 90% of their breakup velocity. It is expected that a fast and solid-body-type rotation flattens the star, causing a gravitational darkening of the stellar surface due to the variation of the temperature and density distribution from the poles to the equator. For Be stars, we therefore have to account for these effects on the stellar spectra and, consequently, on the determination of the fundamental parameters. In the present paper, these effects are introduced as corrections (see Step 3 of Fig. 2) directly applied to the fundamental parameters derived in the two previous steps (Sect. 4.1 and 4.2). These corrections were estimated by assuming different rotation rates and by systematically comparing a grid of spectra taking into account the effects of fast rotation (Frémat et al. 2004; Frémat et al. 2005) to a grid of spectra computed using usual plane-parallel model atmospheres (see Sect. 3). Eventually, the complete procedure provides us with the parameters of the stellar *parent non-rotating counterpart* (i.e. parameters that the stars would have if they were rotationless), further called *pnrc* parameters, estimated at different Ω/Ω_c values. It is the value of these *pnrc* parameters that should be preferred to interpret and discuss the future COROT data.

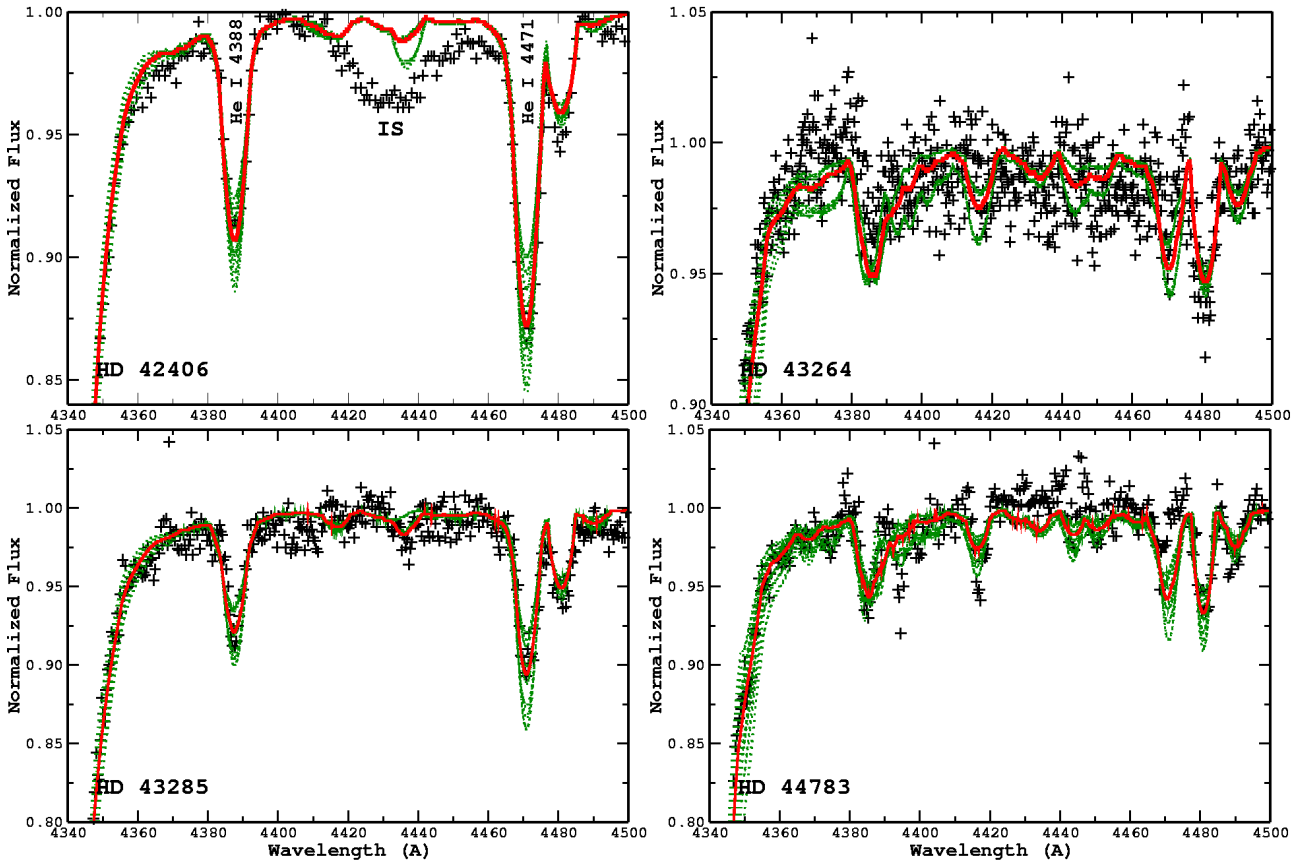

Fig. 3. Comparison between observed data (crosses) and fitted synthetic spectra (full line) in a spectral domain containing the red wing of the Hγ line and 2 neutral helium lines. Dotted lines are used to represent 26 spectra computed for different combinations (i.e. there are in fact 3^3 spectra or stellar parameters combinations, but one of them corresponds to the best fit we obtained) of the upper and lower limits of the $T_{\rm eff}$, log g, and $V \sin i$ values adopting the error bars given in Table 4.

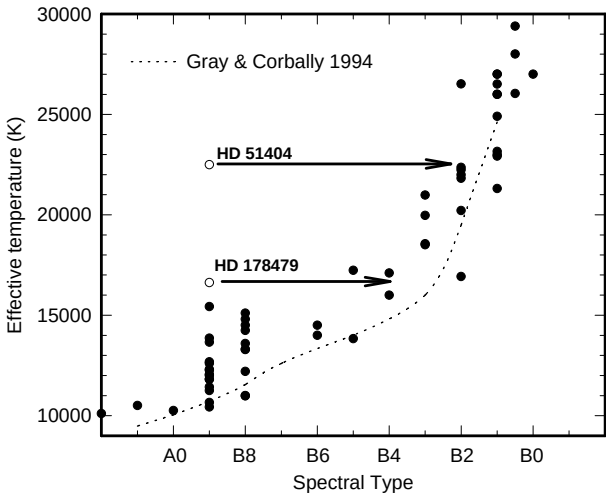

Fig. 4. Veiling corrected apparent effective temperatures listed in Table 4 are reported versus their spectral type given in SIMBAD (filled circles) and compared to the calibration obtained by Gray & Corbally (1994) for dwarf stars (dashed line).

5. Results

The procedure described in Sect. 3 was applied to the sample of selected Be stars (Table 1). We show in Fig. 3 an example of observed and fitted-synthetic spectra limited to a small part of the considered spectral domain. A more complete comparison performed for all the studied stars is available as a postscript file, which can be downloaded from the CDS. In the same figure, we also plotted with dotted lines 26 synthetic spectra computed for different combinations (i.e. 3^3 spectra or combinations, one of them corresponding to the best fit we obtained) of the upper and lower limits of the $T_{\rm eff}$, log g, and $V \sin i$ values adopting the error bars given in Table 4.

We plot in Fig. 4 the apparent value of the effective temperature we derived against the spectral type available in the SIMBAD database. This enables us to compare our determinations with older measurements and to detect any inconsistency (i.e. HD 51404 and HD 184479). Such a comparison is useful since, as far as the hydrogen and neutral helium lines are considered, the apparent stellar parameters characterize the spectrum fairly well (e.g. see Fig. 9 in Frémat et al. 2005) and can therefore be directly related to the spectral type given in SIMBAD. Taking into account the fact that our sample also includes stars that have luminosity classes generally ranging

from III to V, the distribution of points fairly follows the effective temperature calibration proposed by Gray & Corbally (1994) for dwarf stars (dashed line in Fig. 4). Table 4 gathers the derived apparent fundamental parameters: cols. 1 and 2 identify the target; cols. 3 and 4 respectively give the V magnitude and spectral type extracted from the SIMBAD database; cols. 5, 6, 7 and 8 list the effective temperature ($T_{\rm eff}$), surface gravity ($\log\ g$), projected rotation velocity ($V\sin i$) and spectral type we obtained; values found in cols. 9 and 10 are estimates of the Hγ line-emission and continuum veiling due to the presence of the circumstellar envelope; col. 10 summarizes previous fundamental parameter determinations. The spectral type we give in col. 8 is an estimate based on the fundamental parameters combined to the $T_{\rm eff}$ and $\log\ g$ calibrations proposed by Gray & Corbally (1994) and by Zorec (1986). Note that, at this stage, our results do not account for stellar flattening and gravitational darkening, but only for veiling. The derived stellar parameters may therefore be considered as veiling-corrected *apparent* values. We computed the luminosity of each target combining these apparent $T_{\rm eff}$ and $\log\ g$ determinations to the theoretical evolutionary tracks of Schaller et al. (1992, Z=0.02). Their position in the HR diagram is plotted in Fig. 8a. Luminosity accuracy is estimated from the $T_{\rm eff}$ and $\log\ g$ error-boxes.

The magnitude of the uncertainty introduced by the fast-rotation effects was estimated by applying the approach detailed in Sect. 4.3 (see also Frémat et al. 2005) and by assuming different $\Omega/\Omega_{\rm c}$ ratios (where Ω and $\Omega_{\rm c}$ respectively are the actual and break-up angular velocities). Rotation corrected fundamental parameters ($T^{\rm o}_{\rm eff}$, $\log g_{\rm o}$ and $V\sin i_{\rm true}$), i.e. *pnrc* parameters, and corresponding inclination angles, *i*, are given in Table 5 for $\Omega/\Omega_{\rm c}$ = 0.8, 0.9, 0.95, and 0.99.

6. Remarks about specific targets

6.1. HD 43264

The Be nature of HD 43264 was first noted by Neiner et al. (2005). However, the surface gravity we derive from the study of the hydrogen and helium lines is quite low ($\log\ g$ = 2.76), which means that the target could be a bright giant. The star is known as a binary in the HIPPARCOS catalogue, probably SB1 considering the magnitude difference between the primary and secondary components (ΔV = V $-$ V = -2.85).

6.2. HD 46380, HD 50087

The observed spectra we used to derive the fundamental parameters of HD 46380 and HD 50087 are very noisy, and thus the parameters are uncertain.

6.3. HD 50138

HD 50138 has a variable shell and is also considered as a B[e] star, whose evolutionary status is very difficult to establish. Several hints (Lamers et al. 1998) suggest that the star could probably be a massive Herbig Be star with an accreting circumstellar disk, i.e. in a pre-main sequence. The spectrum is very complex with strong emission lines and thin absorption features superimposed on the photospheric lines. The determination of fundamental parameters from the fit of the spectrum is therefore very difficult and could be inaccurate.

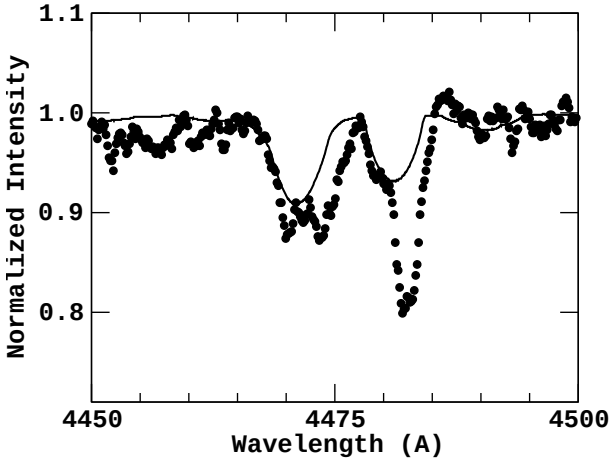

Fig. 5. Observed (dots) and fitted (solid line) He 4471 and Mg 4481 lines in the spectrum of HD 55806.

6.4. HD 51404

HD 51404 is a poorly studied object recognized as Be star by Merrill & Burwell (1949) and erroneously classified as a B9 V star. Our determinations clearly show that its spectral type is B1.5, as can be deduced from Fig. 4 and from the strength of the He spectral lines.

6.5. HD 52721

HD 52721 is also known as a Herbig Ae/Be candidate (Vieira et al. 2003) and is a member of a visual double system with angular separation ~ 0.65 arcsec (Perryman et al. 1997). Though a fair agreement between observed and theoretical fitted spectra is observed, the $V\sin i$ value we derive (352 km s^{-1}) strongly deviates from those obtained in previous works: 243 ± 93 km s^{-1}(Yudin 2001) and 456 km s^{-1}(Halbedel 1996).

6.6. HD 55806

HD 55806 is a poorly studied B type star that was found to have bright emission lines by Merrill & Burwell (1949). We were not able to find any set of fundamental parameters allowing to simultaneously fit the observed helium and magnesium spectral lines (see Fig. 5). As a matter of fact, all the helium lines in the studied spectral range show unusual line-shapes probably related to the presence of a close companion.

6.7. HD 178479

Only two publications are found in SIMBAD for HD 178479, which is classified B9 V. The strength of the He spectral lines is however much too large for a late B-type star and rather corresponds to a B3 star (see Fig. 4).

Table 4. Veiling corrected apparent stellar parameters. ID numbers, SIMBAD V magnitudes and spectral types are given for each target in cols. 1, 2, 3 and 4. The derived stellar parameters (effective temperature, surface gravity, and $V\sin i$) are gathered in cols. 5, 6 and 7. Their accuracy is estimated by scanning the solutions space while adopting different initial values for the parameters. Spectral types (col. 8) are derived from the apparent stellar parameters combined to the $T_{\rm eff}$ and log g calibrations proposed by Gray & Corbally (1994) and by Zorec (1986). Cols. 9 and 10 list the equivalent width of the Hγ emission components and the estimates of the veiling correction, respectively. The error bars on the equivalent widths are generally of the order of 15% and are a product of the fitting process. Errors on the veiling parameter, r, are estimated by accounting for the accuracy on $W_\lambda^{H\gamma}$ and by assuming a 95% confidence interval on the reference data of Ballereau et al. (Fig. 9a, 1995).

ID		SIMBAD		This work					
HD/BD	HIP/BD/ MWC	V	Sp. Type	$T_{\rm eff}$ (K)	log g (c.g.s.)	V sin i (km s^{-1})	Sp. Type	$W_\lambda^{H\gamma}$ (mÅ)	r
42406	29298	8.01	B9	15400±1000	3.72±0.10	300±25	B4 IV	0.30±0.05	–
43264	29719	7.51	B9	10500±1000	2.76±0.10	288±10	B9 III	0.22±0.03	–
43285	29728	6.05	B6Ve	14000±1000	3.78±0.10	260±20	B5 IV	0.21±0.03	–
44783	30448	6.225	B8Vn	11000±1000	3.05±0.15	226±50	B9 III	0.10±0.02	–
45901	30992	8.87	B2Ve	26500±2000	3.73±0.15	164±15	B0.5 IV	0.82±0.12	0.17±0.08

... A complete version of the table is available at the CDS

Table 5. Sample of fundamental parameters corrected for the effects of fast rotation at different Ω/Ω_c ratios. Error bars on the parameters are of the same order as in Table 4. When the projected rotation velocity is greater than the break-up speed or equatorial speed, the Table is left blank.

	$\Omega/\Omega_c = 0.80$				$\Omega/\Omega_c = 0.90$				$\Omega/\Omega_c = 0.95$				$\Omega/\Omega_c = 0.99$			
HD	$T^o_{\rm eff}$ (K)	$\log g_o$ (cgs)	$V\sin i_{\rm true}$ (km s^{-1})	i (°)	$T^o_{\rm eff}$ (K)	$\log g_o$ (cgs)	$V\sin i_{\rm true}$ (km s^{-1})	i (°)	$T^o_{\rm eff}$ (K)	$\log g_o$ (cgs)	$V\sin i_{\rm true}$ (km s^{-1})	i (°)	$T^o_{\rm eff}$ (K)	$\log g_o$ (cgs)	$V\sin i_{\rm true}$ (km s^{-1})	i (°)
42406									16500	3.96	338	61	17000	3.97	360	79
43264													12000	3.16	284	79
43285	15000	4.03	266	71	15000	3.99	274	55	15000	3.95	292	51	15000	3.93	309	58
44783	12000	3.37	226	93	12000	3.40	227	80	11500	3.13	231	82	11500	3.21	218	57
45901	27000	3.78	171	31	27000	3.79	173	26	27500	3.84	175	24	29500	4.06	174	21

... A complete version of the table is available at the CDS

6.8. HD 179343

Thin features superimposed on broader spectral lines are detected in the spectra of HD179343, which is considered as a Be shell star. It is however interesting to note that it is also known as a "single-entry" binary in the HIPPARCOS catalogue with $\Delta V = 0.481$. The shell features could therefore be an artifact of the secondary component.

6.9. HD 184279

HD 184279 is an early B-type star showing numerous variable shell absorptions superimposed on the photospheric spectrum (Ballereau & Chauville 1989), as can be noticed from Fig. 1 where the equivalent widths of the He 4471 and Mg 4481 lines are clearly overestimated. Since these features are also affecting the helium lines (i.e. our main temperature and $V\sin i$ criteria), the fitting zones were adapted to exclude the features as well as possible.

7. Discussion

7.1. Effects of veiling correction

Be stars showing strong Hγ emission were corrected using an empirical approach described by Ballereau et al. (1995) (see Sect. 4.2). Including such veiling corrections in the calculations often produces a lowering of the observed continuum and, consequently, a spectral line strengthening. From this procedure, different $T_{\rm eff}$ and higher log g values are generally obtained, which leads, in the HR diagram, to pull the location of the Be stars towards the ZAMS (see Fig. 6).

7.2. Effects of fast rotation

In our sample, the effects of fast rotation on effective temperature, surface gravity and projected rotation velocity are generally significant when $V\sin i > 150$ km s^{-1}. As expected, accounting for these effects provides higher values of the *pnrc* fundamental parameters (e.g. average $V\sin i$ in Table 6). We further note from Table 5 that, for $\Omega/\Omega_c \geq 0.8$ and if we except $V\sin i_{\rm true}$, the pnrc stellar parameters generally do not vary significantly with Ω/Ω_c. This is mainly due to the fact that, at a

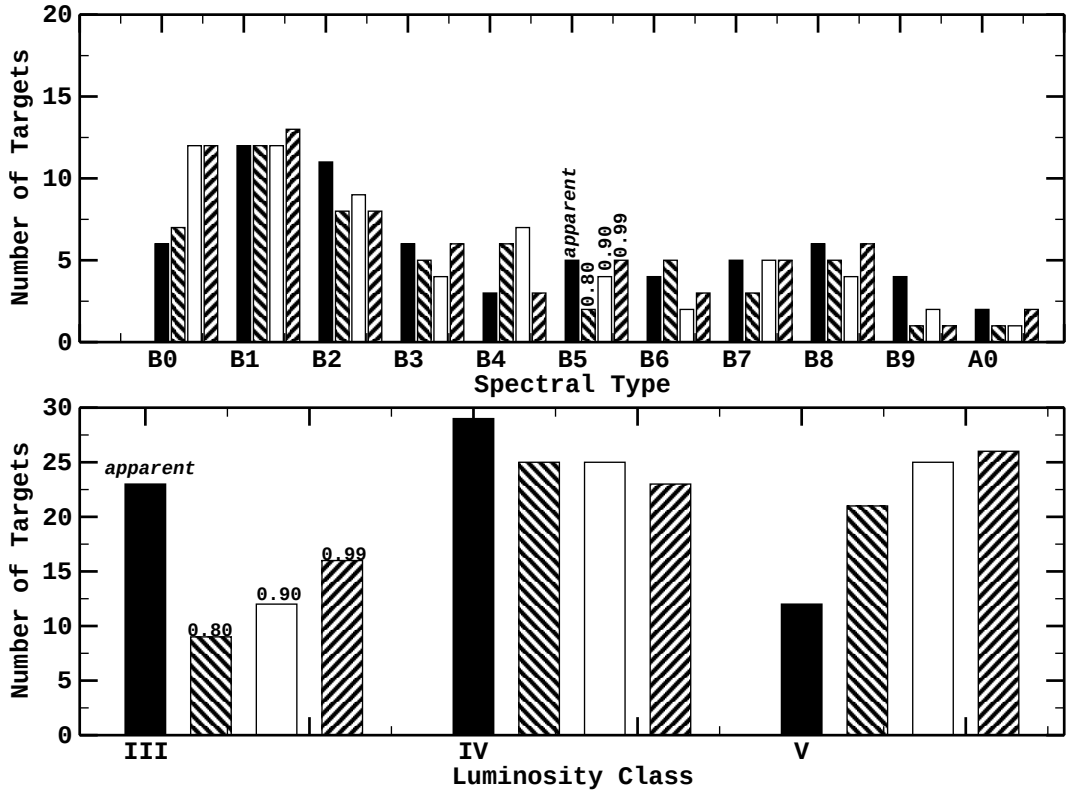

Fig. 7. Histogram showing the changes in spectral type and luminosity class distribution when including the effects of stellar flattening and gravitational darkening. *Apparent* spectral types and luminosity classes are represented with filled bars, while other bars give the corrected ones adopting Ω/Ω_c= 0.80, 0.90, 0.99.

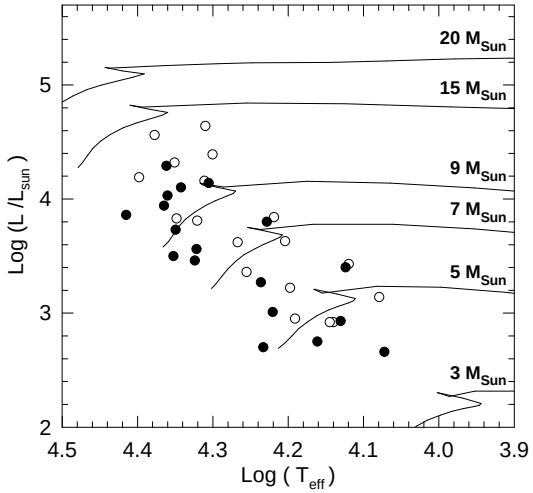

Fig. 6. Location of Be stars showing the strongest Hγ emission in the HR diagram with (filled circles) and without (open circles) accounting for the veiling effects. Theoretical evolutionary tracks are taken from Schaller et al. (1992) for a solar-like metallicity.

fixed $V\sin i$ value, the increase of Ω/Ω_c leads to smaller inclinations and, consequently, leads to explore regions of the stellar surface that are less affected by the flattening of the star. Since a recent study (Frémat et al. 2005) showed that Be stars are found to rotate, on average, at $\Omega/\Omega_c\sim$ 0.88 when properly

Table 6. Average $V\sin i$ in km s^{-1} computed assuming different Ω/Ω_c towards the Galactic centre and anticentre. For each value of Ω/Ω_c, only a certain number of stars (given in brackets) have a reasonable model (see Table 5) and could be used in the computation.

Ω/Ω_c	Anticentre B9–B0	Centre B9–B0
0.80	221±65 (27)	188±75 (27)
0.90	236±75 (29)	216±79 (30)
0.95	251±84 (31)	223±82 (30)
0.99	260±92 (32)	235±84 (31)

treating fast rotation effects, uncertainties on the actual value of the angular velocity are not expected to carry too high errors on the estimate of the *pnrc* $T_{\rm eff}^{\rm o}$ and $\log g_{\rm o}$ parameters.

From Fig. 7, we see that the effects of fast rotation also appear on the targets spectral type and luminosity class. As already mentioned by Briot & Zorec (1994), the top of the spectral type distribution of Be stars is centered on B1 (instead of B2) when gravitational darkening and stellar flattening are taken into account. It is worth recalling, that the luminosity class of Be stars are even more sensitive to these effects, which shift the targets toward lower luminosities when they are included in the computations. In view of these results, and keeping in mind that the veiling effect makes this situation even

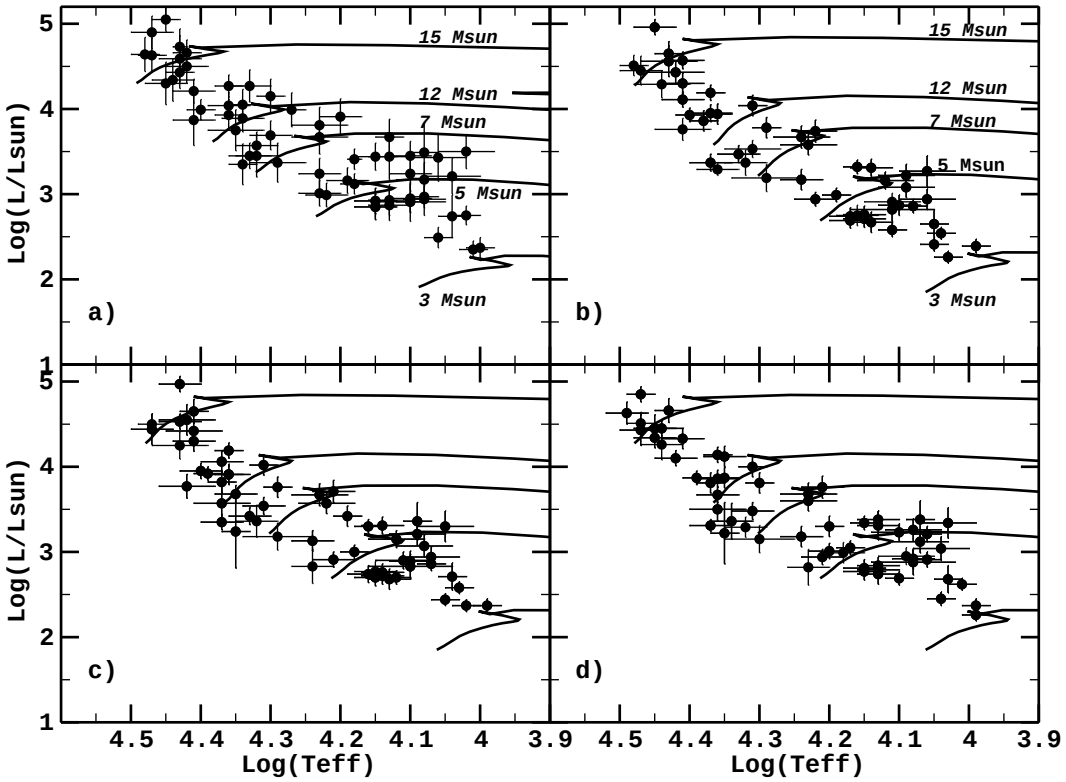

Fig. 8. Panel a): Location of the Be stars (filled circles) in the HR diagram adopting the veiling-corrected apparent stellar parameters of Table 4. Theoretical evolutionary tracks (lines) are taken from Schaller et al. (1992) and adapted following a procedure given by Zorec et al. (2005). Panels b), c) and d): Location of the Be stars (filled circles) in the HR diagram accounting for gravitational darkening effects and assuming Ω/Ω_c = 0.80, 0.90, and 0.99, respectively. Theoretical evolution tracks (lines) take into account the effects of fast rotation as described by Meynet & Maeder (2000). The effective temperature and the luminosity reported in the figures are therefore surface-averaged quantities (Table 7).

Table 7. Sample of the *pnrc* surface-*averaged* parameters and of the respective interpolated masses $M/M_\odot$, ages τ, and fractional ages $\tau/\tau_{\rm MS}$. When the projected rotation velocity was greater than the break-up speed or than the equatorial speed, the Table were left blank.

HD	$T_{\rm eff}^{\rm surf.}$	log $g^{\rm surf.}$	log $L/L_\odot$ $^{\rm surf.}$	M/M$_\odot$	age (years)	$\tau/\tau_{\rm MS}$
			Ω/Ω_c = 0.80			
42406						
43264						
43285	14500±1100	4.02±0.17	2.69± 0.09	4.60± 0.30	6.6E+07±2.0E+07	0.47± 0.13
44783	11500±1100	3.33±0.21	2.94± 0.12	4.30± 0.30	1.7E+08±1.5E+07	1.02± 0.03
45901	26000±2300	3.74±0.21	4.43± 0.13	13.60± 1.30	1.2E+07±2.0E+06	0.75± 0.10
46380	23000±1100	3.88±0.14	3.94± 0.12	10.00± 0.60	1.7E+07±2.6E+06	0.62± 0.09
46484	27000±1000	3.64±0.13	4.65± 0.14	15.70± 1.30	1.1E+07±6.0E+05	0.80± 0.04
47054	12500± 800	3.58±0.15	2.87± 0.12	4.60± 0.20	1.3E+08±1.1E+07	0.91± 0.05
47160	11500± 600	3.74±0.11	2.41± 0.08	3.60± 0.10	2.1E+08±1.7E+07	0.79± 0.05
47359						
49330	26000±1700	3.84±0.17	4.30± 0.12	12.80± 1.00	1.2E+07±1.9E+06	0.69± 0.10
... A complete version of the table is available at the CDS						

worse, it seems that luminosity classes are very inaccurate in characterizing the evolutionary status of Be stars.

7.3. Evolutionary status of Be stars

The knowledge of whether the Be phenomenon is an innate property of the stars or whether it depends on stellar evolution is a matter of great interest to better understand the precise nature of Be stars and its potential link with asteroseismology.

A recent study (Zorec et al. 2005) performed on a large sample of field Be stars (i.e. 97 Be stars) uniformly spread over the whole sequence of B type stars showed that the appearance of the Be phenomenon for the lower mass stars generally occurs during the second half of the main sequence life time ($\tau_{\rm MS}$), but that it appears earlier at greater stellar masses. In order to see if there is such a trend in our sample of Be stars, we derive their masses, ages and luminosity using an interpolation procedure developed by Zorec et al. (2005), which accounts for the changes introduced by fast rotation in the evolutionary tracks (Heger & Langer 2000; Meynet & Maeder 2000, 2002; Maeder & Meynet 2001). Since these modeled evolutionary tracks are given in terms of surface-*averaged* effective temperatures and bolometric luminosities, we transformed the *pnrc* parameters into surface-*averaged* ones using the angular velocity ratios $\Omega/\Omega_{\rm c}$ = 0.80, 0.90, and 0.99. The *pnrc* surface-*averaged* parameters and the respective interpolated masses $M/M_{\odot}$, ages τ, and fractional ages $\tau/\tau_{\rm MS}$ are given in Table 7. Fig. 8a shows the HR diagram of the program stars depicted by the veiling-corrected *apparent* $T_{\rm eff}$ and $\log L/L_{\odot}$ values and evolutionary tracks for non-rotating stars (Schaller et al. 1992). Fig. 8b, 8c, and 8d show the HR diagram of the program stars in terms of surface-*averaged* fundamental parameters assuming the stars rotate at $\Omega/\Omega_{\rm c}$ = 0.80, 0.90, and 0.99 respectively. The corresponding evolutionary tracks (Fig. 8b, 8c, and 8d) were calculated for the ZAMS equatorial rotation velocity V_o = 300 km s^{-1}. Note that $\Omega/\Omega_{\rm c}$ = 0.90 represents the average angular velocity rate of galactic field Be stars (Frémat et al. 2005). It must also be noted that if a star starts its evolution on the ZAMS as a rigid rotator with a rotation velocity V_o, as a consequence of the initial angular momentum redistribution, the surface velocity decreases somewhat in a lapse of time ranging from 1 to 2% (Denissenkov et al. 1999) of the stellar $\tau_{\rm MS}$. Since, on one hand, we do not know the actual initial velocity of the sample stars on the ZAMS and, on the other hand, dwarf Be stars have a very flat distribution of their equatorial true rotational velocities versus the spectral type around $V \sim 300$ km s^{-1} (Yudin 2001; Zorec et al. 2004, Fig. 1b), the comparisons done above with evolutionary tracks calculated for V_o = 300 km s^{-1} are realistic (Meynet & Maeder 2000).

Fig. 9 shows the average $\tau/\tau_{\rm MS}$ ratios we computed for each star assuming $\Omega/\Omega_{\rm c}$ = 0.90. Most of the Be stars are found, on the average, in the second half of the main sequence life time and we clearly observe a paucity of very young Be stars at masses lower than 6 $M_{\odot}$. The lack of low mass Be stars ($M < 7M_{\odot}$) in the first half of the main sequence was noted in other recent works that deal with independent stellar samples. Using a magnitude-limited sample (97 Be stars) that mirrors the distribution of all known Be stars in the Bright Stars Catalogue (Hoffleit & Warren 1991), Zorec et al. (2005) obtained a void of low mass Be stars in the first half of the main sequence evolutionary phase. An equivalent conclusion was also obtained by Levenhagen (2004) from a study of 130 Be stars with visual magnitudes ranging from 7 to 9 mag. In our case, probably due to the fact that the sample is smaller and the stars are not uniformly distributed over the mass range that defines B-type stars, the trend is mainly obvious at masses $< 6M_{\odot}$. However, since the same result also repeats in other studies, we think that this effect can be hardly related to some sampling bias.

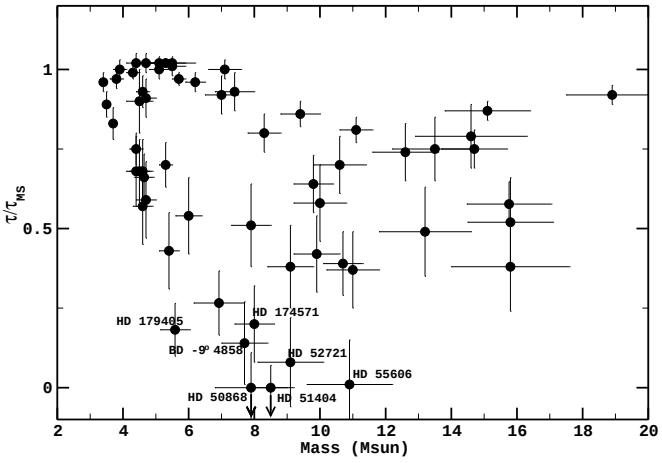

Fig. 9. $\tau/\tau_{\rm MS}$ ratios of the program Be stars as a function of stellar mass (see Table 7). The ratios and masses are computed for $\Omega/\Omega_{\rm c}$ = 0.90, which corresponds to the expected average angular velocity of Be stars.

Furthermore, if we exclude the targets with low S/N spectra, 5 stars (HD 50868, HD 51404, HD 52721, HD 174571, BD -9^{o}4858) are obviously much younger than the rest of the sample (Fig. 9) and might be considered as Herbig Ae/Be candidates, as is already the case for HD 174571 (Vieira et al. 2003).

7.4. Be stars as COROT targets

Fields to be observed with COROT have already been preselected based on the parameters of the potential targets. Only Be stars located in these fields can still be chosen as secondary targets and would then be observed for about 5 consecutive months. Table 8 summarizes these Be stars that are candidates as secondary targets. Whether all these fields will be observed with COROT will depend on the length of the mission; at least five of them will be observed. Moreover, since COROT tries to sample as well as possible the HR diagram, not all the secondary Be candidates in a selected field will eventually be observed with COROT. The choice will be made according to technical constraints of the satellite and to the stellar parameters determined in this paper.

Be stars that will not be observed in a long run, either because they are not located in one of the selected fields (and therefore are not listed in Table 8) or because they are not chosen as a secondary target in these fields, can be proposed as targets for short runs lasting 20-30 days. Again the choice of these Be short-run targets will depend on the fundamental parameters determined in this paper, and on their variability. In particular HD 168797 seems to be a prime candidate for a short-run (see Gutiérrez-Soto et al. 2005).

8. Conclusions

In this paper, we determined the fundamental parameters (spectral type, effective temperature, surface gravity and projected

Table 8. Be stars close to primary COROT target candidates, which could be selected as secondary targets.

	Galactic Centre		
Be Secondary	V	Sp. Type	COROT Field
HD 171219	7.65	B5 III	HD 171234 & HD 170580
HD 171219	7.65	B5 III	HD 171834
HD 175869	5.56	B8 III	HD 175726
HD 181231	8.58	B5 IV	HD 181555 & HD 180642
	Galactic Anticentre		
Be Secondary	V	Sp. Type	COROT Field
HD 43285	6.05	B5 IV	HD 43587
HD 43913	7.88	A0	HD 43587
HD 45901	8.87	B0.5 IV	HD 46558
HD 46484	7.65	B0.5 IV	HD 46558
HD 47359	8.87	B0 IV	HD 46558
HD 49330	8.95	B0.5 IV	HD 49933 & HD 49434
HD 49567	6.15	B3 III	HD 49933 & HD 49434
HD 49585	9.13	B0.5 IV	HD 49933 & HD 49434
HD 50087	9.08	B8 III	HD 49933 & HD 49434
HD 50209	8.36	B8 IV	HD 49933 & HD 49434
HD 50891	8.88	B0.5 V	HD 52265
HD 51193	8.06	B1.5 IV	HD 52265
HD 51404	9.30	B1.5 V	HD 52265
HD 51452	8.08	B0 IV	HD 52265

rotation velocity) for the Be stars that can be observed in COROT's seismology fields. To this end, a careful and detailed modeling of the stellar spectra was applied, accounting for NLTE effects as well as for the effects due to fast rotation (stellar flattening and gravitational darkening). On the average, the uncertainties we obtained on the stellar parameters are of the order of 10 % on $V \sin i$, 7 % on $T_{\rm eff}$, and 3.3 % on $\log L/L_{\odot}$. Our results are therefore very well suited for the target selection of COROT Be stars and, further, will also be very useful when analyzing the huge amount of data that COROT will provide.

A study of the fast rotation effects, as well as of those related to circumstellar veiling, on the spectral type and luminosity class distribution shows that the luminosity class of Be stars is generally inaccurate in characterizing their evolutionary status. Evolutionary tracks for fast rotators were further used to derive stellar masses and ages in order to discuss the appearance of the Be phenomenon with respect to the evolutionary status of the stars. Most of the Be stars of our sample are found in the second half of the main sequence life time. There is further an obvious lack of very young Be stars at masses lower than 6 $M_{\odot}$ which reproduces previous observations made by Zorec et al. (2005) and Levenhagen (2004).

Finally, we give a preliminary list of the Be stars that could be chosen as secondary targets for the COROT mission. The fundamental stellar parameters we derived will be further used to carry on the secondary target selection procedure, as well as to determine which object could be proposed for short runs.

Acknowledgements. We wish to acknowledge the referee, D. Baade, for his suggestions which greatly improved the readability of the paper. We thank J.Gutiérrez–Soto for his remarks. We are grateful to the ground-based asteroseismology working group of COROT and all the contributors of GAUDI. This research has made use of the SIMBAD database maintained at CDS, Strasbourg, France. YF thanks Dr. P.Lampens for hosting him at the Royal Observatory of Belgium. JRM acknowledges continuous financial support of the CNPQ Brazilian Agency.

References

Abt, H. A., Levato, H., & Grosso, M. 2002, ApJ, 573, 359
Baglin, A., Auvergne, M., Catala, C., et al. 2002, in ASP Conf. Ser. 259: IAU Colloq. 185: Radial and Nonradial Pulsations as Probes of Stellar Physics, 626
Ballereau, D. & Chauville, J. 1989, A&A, 214, 285
Ballereau, D., Chauville, J., & Zorec, J. 1995, A&AS, 111, 423
Briot, D. & Zorec, J. 1994, in IAU Symp. 162: Pulsation; Rotation; and Mass Loss in Early-Type Stars, 356
Chauville, J., Zorec, J., Ballereau, D., et al. 2001, A&A, 378, 861
Cidale, L., Zorec, J., & Tringaniello, L. 2001, A&A, 368, 160
Conti, P. S. & Ebbets, D. 1977, ApJ, 213, 438
Cunto, W., Mendoza, C., Ochsenbein, F., & Zeippen, C. J. 1993, A&A, 275, L5
Denissenkov, P. A., Ivanova, N. S., & Weiss, A. 1999, A&A, 341, 181
Floquet, M., Neiner, C., Janot-Pacheco, E., et al. 2002, A&A, 394, 137
Frémat, Y., Zorec, J., Hubert, A. M., et al. 2004, in IAU Symposium, 23–+
Frémat, Y., Zorec, J., Hubert, A.-M., & Floquet, M. 2005, A&A, in press, astroph/0503381
Gray, R. O. & Corbally, C. J. 1994, AJ, 107, 742
Grevesse, N. & Sauval, A. J. 1998, Space Science Reviews, 85, 161
Gulati, R. K., Malagnini, M. L., & Morossi, C. 1989, A&AS, 80, 73
Gutiérrez-Soto, J., Fabregat, J., Suso, J., et al. 2005, A&A, in preparation
Halbedel, E. M. 1996, PASP, 108, 833
Heger, A. & Langer, N. 2000, ApJ, 544, 1016
Hoffleit, D. & Warren, J. W. H. 1991, The Bright Star Catalogue, 5th Revised Ed. (Astronomical Data Center, NSSDC/ADC)
Hubeny, I. & Lanz, T. 1995, ApJ, 439, 875
Hubert, A. M. & Floquet, M. 1998, A&A, 335, 565
Jaschek, M., Slettebak, A., & Jaschek, C. 1981, Be stars Newsletter, 4, 9
Kurucz, R. L. 1993, Kurucz CD-ROM No.13. Cambridge, Mass.: Smithsonian Astrophysical Observatory.
Lamers, H. J. G. L. M., Zickgraf, F., de Winter, D., Houziaux, L., & Zorec, J. 1998, A&A, 340, 117
Lanz, T. & Hubeny, I. 2003, ApJS, 146, 417
Levenhagen, R. 2004, PhD Thesis (University of Sao Paulo)
Levenhagen, R. S. & Leister, N. V. 2004, AJ, 127, 1176
Lyubimkov, L. S., Rachkovskaya, T. M., Rostopchin, S. I., & Lambert, D. L. 2002, MNRAS, 333, 9
Maeder, A. & Meynet, G. 2001, A&A, 373, 555
Merrill, P. W. & Burwell, C. G. 1949, ApJ, 110, 387
Meynet, G. & Maeder, A. 2000, A&A, 361, 101
Meynet, G. & Maeder, A. 2002, A&A, 390, 561

Neiner, C., Hubert, A.-M., & Catala, C. 2005, ApJS, 156, 237
Neiner, C., Hubert, A.-M., Floquet, M., et al. 2002, A&A, 388, 899
Perryman, M. A. C., Lindegren, L., Kovalevsky, J., et al. 1997, A&A, 323, L49
Porter, J. M. & Rivinius, T. 2003, PASP, 115, 1153
Rivinius, T., Baade, D., Stefl, S., et al. 1998, A&A, 336, 177
Royer, F., Grenier, S., Baylac, M.-O., Gómez, A. E., & Zorec, J. 2002, A&A, 393, 897
Schaller, G., Schaerer, D., Meynet, G., & Maeder, A. 1992, A&AS, 96, 269
Sigut, T. A. A. 1996, ApJ, 473, 452
Slettebak, A. 1982, ApJS, 50, 55
Sokolov, N. A. 1995, A&AS, 110, 553
Solano, E., Catala, C., Garrido, R., et al. 2005, AJ, 129, 547
Theodossiou, E. 1985, MNRAS, 214, 327
Townsend, R. H. D., Owocki, S. P., & Howarth, I. D. 2004, MNRAS, 350
Varosi, F., Lanz, T., de Koter, A., et al. 1995, ftp://idlastro.gsfc.nasa.gov/pub/contrib/varosi/modion
Vieira, S. L. A., Corradi, W. J. B., Alencar, S. H. P., et al. 2003, AJ, 126, 2971
Yudin, R. V. 2001, A&A, 368, 912
Zorec, J. 1986, PhD Thesis: Structure et rotation différentielle dans les étoiles B avec et sans émission (Paris: Université VII, 1986)
Zorec, J., Frémat, Y., & Cidale, L. 2005, A&A, in press
Zorec, J., Levenhagen, R., Chauville, J., et al. 2004, in IAU Symposium, 89–+

ONLINE DATA

Table 1. Spectra used in this study. For the ELODIE spectra, the signal to noise ratio (S/N) was provided by the INTERTACOS (OHP) reduction pipeline, while for the other data it was computed with IRAF by selecting some parts of the continuum in the studied spectral region. '[1]' indicates that the spectrum is available in GAUDI.

HD	Obs. date	T_{exp} (s)	Instrument	S/N
42406	2004-02-05	900	FEROS	249
43264	2001-11-27	3300	ELODIE[1]	83
43285	2001-12-21	1800	ELODIE[1]	123
44783	2000-12-18	1500	ELODIE[1]	121
45901	2004-01-03	2700	AURELIE 4280_G3	120
46380	2001-12-22	3600	ELODIE[1]	53
46484	2003-01-26	3600	ELODIE[1]	107
47054	2002-01-28	300	FEROS[1]	145
47160	2002-01-28	300	FEROS[1]	150
47359	2004-01-03	2400	AURELIE 4280_G3	140
49330	2001-12-22	3600	ELODIE[1]	54
49567	2002-04-01	1500	ELODIE[1]	132
49585	2004-01-07	3600	AURELIE 4485_G2	140
49787	2003-01-18	220	FEROS[1]	126
50083	2003-01-17	1200	ELODIE[1]	96
50138	2003-01-18	110	FEROS[1]	144
50209	2001-12-24	5150	ELODIE[1]	46
50581	2003-01-27	3600	ELODIE[1]	73
50696	2001-12-22	7200	ELODIE[1]	48
50868	2001-10-09	500	FEROS[1]	160
50891	2005-01-05	4500	AURELIE	250
51193	2004-01-03	900	AURELIE 4280_G3	130
51404	2004-01-04	3600	AURELIE 4280_G3	150
51452	2004-01-03	900	AURELIE 4280_G3	126
51506	2003-01-24	3600	ELODIE[1]	89
52721	2004-02-05	300	FEROS	260
53085	2003-01-15	180	FEROS[1]	115
53667	2003-01-18	300	FEROS[1]	105
54464	2004-02-05	1800	FEROS	317
55135	2004-02-05	300	FEROS	250
55606	2001-12-22	5400	ELODIE[1]	40
55806	2004-02-05	1500	FEROS	250
57539	2003-01-17	130	FEROS[1]	72
166917	2002-08-14	720	ELODIE[1]	90
168797	1999-07-25	900	ELODIE[1]	171
170009	2000-06-07	2400	ELODIE[1]	141
170714	2001-07-06	450	FEROS[1]	98
171219	2002-07-07	300	FEROS[1]	130
173219	2001-07-06	450	FEROS[1]	85
173371	2001-07-06	300	FEROS[1]	115
173530	2003-07-18	600	OPD CASS	30
173637	2003-07-18	1200	OPD CASS	50
173817	2003-07-18	600	OPD CASS	70
174513	2004-07-05	2740	AURELIE 4481_G3	170
174571	2004-07-12	3600	AURELIE 4481_G3	180
	2004-07-15	3600	AURELIE 4100_G3	200

HD	Obs. date	T_{exp} (s)	Instrument	S/N
174705	2004-07-05	2400	AURELIE 4481_G3	140
	2004-07-15	3600	AURELIE 4100_G3	140
174886	2002-07-07	300	FEROS[1]	80
175869	2001-07-07	150	FEROS[1]	90
176159	2004-07-20	2500	AURELIE 4481_G3	190
176630	2001-07-07	1800	ELODIE[1]	94
	2001-07-06	600	FEROS[1]	100
178479	2004-07-21	3600	AURELIE 4481_G3	180
179343	2003-07-18	400	OPD CASS	120
179405	2004-07-04		AURELIE 4481_G3	
180126	2004-07-04	1000	AURELIE 4481_G3	320
	2004-07-13	2700	AURELIE 4100_G3	170
181231	2003-07-18	1000	OPD CASS	60
181308	2003-07-18	700	OPD CASS	70
181367	2003-07-18	1000	OPD CASS	50
181709	2004-07-20	2000	AURELIE 4481_G3	180
181803	2004-07-19	3600	AURELIE 4481_G3	125
184279	2002-07-06	300	FEROS[1]	40
	2003-07-18	500	OPD CASS	100
184767	2004-07-18	1000	AURELIE 4481_G3	110
194244	1999-12-20	3600	ELODIE[1]	112
230579	2004-07-05	3600	AURELIE 4481_G3	130
BD-09°4858	2004-07-20	2400	AURELIE 4481_G3	180

Table 4. Veiling corrected apparent stellar parameters. ID numbers, SIMBAD V magnitudes and spectral types are given for each target in cols. 1, 2, 3 and 4. The derived stellar parameters (effective temperature, surface gravity, and $V \sin i$) are gathered in cols. 5, 6 and 7. Their accuracy is estimated by scanning the solutions space while adopting different initial values for the parameters. Spectral types (col. 8) are derived from the apparent stellar parameters combined to the $T_{\rm eff}$ and log g calibrations proposed by Gray & Corbally (1994) and by Zorec (1986). Cols. 9 and 10 list the equivalent width of the Hγ emission components as well as the estimates of the veiling correction, respectively. The error bars on the equivalent widths are generally of the order of 15% and are a product of the fitting process. Errors on the veiling parameter, r, are estimated by accounting for the accuracy on $W_\lambda^{H\gamma}$ and by assuming a 95% confidence interval on the reference data of Ballereau et al. (Fig. 9a, 1995). Previous determinations of the stellar parameters are given in col.11 and are taken from: (1) Royer et al. (2002); (2) Sokolov (1995); (3) Abt et al. (2002); (4) Yudin (2001); (5) Levenhagen & Leister (2004); (6) Chauville et al. (2001); (7) Lyubimkov et al. (2002); (8) Gulati et al. (1989); (9) Zorec (1986); (10) Halbedel (1996); (11) Cidale et al. (2001); (12) Conti & Ebbets (1977); (13) Theodossiou (1985); (14) Slettebak (1982).

ID		SIMBAD		This work						
HD/BD	HIP/BD/ MWC	V	Sp. Type	$T_{\rm eff}$ (K)	log g (c.g.s.)	V sin i (km s^{-1})	Sp. Type	$W_\lambda^{H\gamma}$ (mÅ)	r	Notes
42406	29298	8.01	B9	15400±1000	3.72±0.10	300±25	B4 IV	0.30±0.05	–	
43264	29719	7.51	B9	10500±1000	2.76±0.10	288±10	B9 III	0.22±0.03	–	
43285	29728	6.05	B6Ve	14000±1000	3.78±0.10	260±20	B5 IV	0.21±0.03	–	$V \sin i$ = 235 km s^{-1} (3) $V \sin i$ = 260 ± 12 km s^{-1} (4) $T_{\rm eff}$ = 16600 ± 600 km s^{-1} (5) log g = 4.0 ± 0.1 (5) $V \sin i$ = 237 ± 11 km s^{-1} (5)
44783	30448	6.225	B8Vn	11000±1000	3.05±0.15	226±50	B9 III	0.10±0.02	–	$V \sin i$ =230 km s^{-1} (3)
45901	30992	8.87	B2Ve	26500±2000	3.73±0.15	164±15	B0.5 IV	0.82±0.12	0.17±0.08	
46380	31199	8.05	B2Vne	22000±1000	3.70±0.15	300±15	B1.5 IV	0.91±0.14	0.20±0.08	$T_{\rm eff}$ =21200 ± 650 K (5) log g =3.5 ± 0.1 (5) $V \sin i$ = 293 ± 3 km s^{-1} (5) $V \sin i$ = 262 km s^{-1} (4)
46484	31305	7.65	B1V	27000±900	3.60±0.15	120±20	B0.5 IV	0.15±0.02	–	
47054	31583	5.57	B8Ve	12000±700	3.40±0.15	222±6	B7 III	0.30±0.05	–	$V \sin i$ = 220 km s^{-1} (3) $V \sin i$ = 226 km s^{-1} (4) $T_{\rm eff}$ = 11995 K (6) log g = 3.9 (6) $V \sin i$ = 230 km s^{-1} (6)
47160	31629	7.104	B9	11500±500	3.70±0.10	149±5	B8 IV	0.07±0.01	–	
47359	+05°1340	8.87	B0.5Vpe...	29500±2000	3.65±0.15	443±40	B0 IV	0.41±0.06	–	
49330	32586	8.95	B0:nnpe	27000±1500	3.82±0.15	270±50	B0.5 IV	0.25±0.04	–	$T_{\rm eff}$ = 27200 ± 600 K (5) log g = 4.0 ± 0.1 (5) $V \sin i$ = 200 ± 10 km s^{-1} (5)
49567	32682	6.146	B3II-III	17000±1500	3.48±0.12	85±10	B3 III	0.23±0.03	–	$V \sin i$ = 75 km s^{-1} (3) $T_{\rm eff}$ = 16600 ± 500 K (7) log g = 3.31 ± 0.19 (7) $T_{\rm eff}$ = 17300 ± 200 K (8) $T_{\rm eff}$ = 16157 K (9) log g = 2.95 – 3.10 (9)
49585	+00°1624	9.13	B0.5:V:nn	25500±1500	3.87±0.1	310±30	B0.5 IV	0.10±0.02	–	
49787	32766	7.54	B1V:pe	25000±1000	4.01±0.10	160±15	B1 V	0.12±0.02	–	$V \sin i$ = 186 ± 2 km s^{-1} (4) $V \sin i$ = 180 ± 2 km s^{-1} (10)
50083	32947	6.92	B2Ve	20000±1000	3.43±0.15	181±20	B2 III	1.33±0.20	0.30±0.11	$V \sin i$ = 178 ± 2 km s^{-1} (4) $V \sin i$ = 170 ± 2 km s^{-1} (10)
50138	32923	6.583	B9	12500±1000	3.25±0.15	60±10	B7 III	–	–	$T_{\rm eff}$ = 13279 ± 100 K (11) log g = 3.4 (11)
50209	32977	8.36	B9Ve	12500±1500	3.50±0.10	200±30	B8 IV	0.62±0.09	0.12±0.07	$T_{\rm eff}$ =12500 ± 450 K (5) log g = 4.00 ± 0.15 (5) $V \sin i$ = 173 ± 15 km s^{-1} (5)
50581	33167	7.54	A0	10250±500	3.60±0.08	240±25	A0 IV	0.30±0.05	–	
50696	+00°1691	8.87	B1:V:nne	21300±1500	3.45±0.15	350±30	B1.5 III	0.28±0.04	–	$T_{\rm eff}$ = 21700 ± 600 K (5) log g = 3.50 ± 0.15 (5) $V \sin i$ = 281 ± 18 (5)
50868	33267	7.85	B2Vne	22000±1000	4.27±0.15	267±20	B1.5 V	0.02±0.01	–	
50891	-03°1643	8.88	B0:pe	27500±2000	3.93±0.20	220±20	B0.5 V	–	–	

ID		SIMBAD		This work						
HD/BD	HIP/BD/ MWC	V	Sp. Type	T_{eff} (K)	log g (c.g.s.)	V sin i (km s^{-1})	Sp. Type	$W_{\lambda}^{H\gamma}$ (mÅ)	r	Notes
51193	33361	8.06	B1V:nn	23000±1000	3.62±0.1	215±25	B1.5 IV	1.35±0.20	0.23±0.11	
51404	-06°1840	9.30	B9	21500±1500	4.15±0.1	335±10	B1.5 V	0.56±0.08	0.10±0.07	
51452	-04°1745	8.08	B0:III:nn	30000±1500	3.88±0.15	298±20	B0 IV	0.23±0.03	–	
51506	33509	7.68	B5	17000±1000	3.84±0.15	172±20	B2.5 IV	0.84±0.13	0.20±0.08	
52721	33868	6.58	B2Vne	22500±2000	3.99±0.20	352±40	B1.5 V	0.59±0.09	0.05±0.07	$V\sin i$ = 456 ± 2 km s^{-1}(10) $V\sin i$ = 243 ± 93 km s^{-1}(4)
53085	34032	7.20	B8	15000±700	3.70±0.10	203±25	B4 IV	0.37±0.06	–	
53667	-08°1734	7.76	B0.5III	28000±1500	3.45±0.10	110±10	B0 III	0.10±0.02	–	$V\sin i$ = 85 km s^{-1} (12)
54464	-03°1762	8.40	B2:V:pe	17000±1500	3.38±0.15	162±15	B2.5 III	0.64±0.10	0.05±0.07	
55135	34719	7.32	B4Vne	17000±1000	4.34±0.20	244±20	B2.5 V	1.20±0.18	0.35±0.10	$V\sin i$ = 258 ± 25 km s^{-1} (4) $V\sin i$ = 270 ± 25 km s^{-1} (10)
55606	-01°1603	9.04	B1:V:nnpe	26000±2000	4.20±0.20	350±60	B0.5 V	1.42±0.21	0.35±0.12	T_{eff} = 28700 ± 550 K (5) log g = 4.1 ± 0.1 (5) $V\sin i$ = 335 ± 20 km s^{-1} (5)
55806	35021	9.10	B9	12500±1000	3.47±0.10	202±15	B7 III	–	–	SB2 (Sect. 6.6)
57539	35669	6.581	B5III	14000±1000	3.30±0.10	141±10	B5 III	0.31±0.05	–	
166917	89242	6.686	B9	12000±1000	3.23±0.15	165±10	B8 III	0.10±0.02	–	$V\sin i$ = 170 ± 7 km s^{-1} (10)
168797	89977	6.147	B3Ve	18500±1000	3.40±0.15	264±20	B2.5 III	0.09±0.01	–	T_{eff} = 21000 K (13) $V\sin i$ = 260 km s^{-1} (3) $V\sin i$ = 251 ± 6 km s^{-1} (4)
170009	90428	8	B8	11000±500	3.40±0.20	180±30	B9 III	0.40±0.06	–	
170714	90768	7.38	B1Vne	23000±1200	3.89±0.15	270±15	B1.5 IV	0.88±0.13	0.15±0.08	
171219	90958	7.65	B8	13500±700	3.07±0.15	300±25	B5 III	-0.20±0.03	–	T_{eff} = 13500 ± 500 K (5) log g = 3.80 ± 0.15 (5) $V\sin i$ = 190 ± 25 km s^{-1} (5)
173219	91946	7.88	B1:V:npe	27000±2000	3.70±0.20	61±10	B0.5 IV	0.80±0.12	0.15±0.08	
173371	91987	6.885	B9III	12500±500	3.50±0.10	295±10	B7 IV	0.29±0.04	–	$V\sin i$ = 291 ± 4 km s^{-1} (4)
173530	+04°3870	8.87	B9	12500±1000	3.10±0.10	250±15	B7 III	0.28±0.04	–	
173637	92128	9.29	B1IV	26500±1500	3.61±0.10	197±20	B1 IV	1.61±0.24	0.40±0.14	$V\sin i$ = 98 ± 10 km s^{-1} (4)
173817	92180	8.65	B8	13500±1000	3.70±0.15	270±15	B6 IV	-0.15±0.02	–	
174513	92510	8.70	B1V:npe	23000±1500	3.80±0.10	251±30	B1.5 IV	0.91±0.14	0.20±0.08	27500 ± 600 K (5) log g = 3.5 ± 0.1 (5) $V\sin i$ = 180 ± 15 km s^{-1} (5) $V\sin i$ = 202 ± 5 km s^{-1} (4) $V\sin i$ = 200 km s^{-1} (10)
174571	92477	8.89	B3V:pe	21000±1500	4.00±0.10	240±15	B1.5 V	0.83±0.12	0.15±0.08	$V\sin i$ =294 ± 19 km s^{-1} (4)
174705	-11°4786	8.34	B2Vne	22000±1500	3.83±0.10	331±25	B1.5 IV	0.05±0.01	–	
174886	92694	7.77	B8	15000±500	3.45±0.10	69±5	B4 III	0.35±0.05	–	
175869	93051	5.563	B9IIIpe...	12000±500	3.38±0.10	167±10	B8 III	0.15±0.02	–	$V\sin i$ = 140 km s^{-1} (3) $V\sin i$ = 120 km s^{-1} (4) T_{eff} = 11066 K (6) log g = 3.48 (6) $V\sin i$ = 175 km s^{-1} (6)
176159	93215	8.98	B9	14000±1000	3.73±0.10	227±15	B5 IV	0.39±0.06	–	$V\sin i$ =218 ± 1 km s^{-1} (4) $V\sin i$ = 220 ± 1 km s^{-1} (10)
176630	93411	7.70	B4IV	16000±1000	3.20±0.15	175±20	B3 III	0.16±0.02	–	
178479	94011	8.92	B9V	16500±1000	3.99±0.10	99±5	B3 V	0.87±0.13	0.15	
179343	94331	6.945	B9	11500±1000	2.97±0.20	148±15	B8 III	0.25±0.04	–	$V\sin i$ = 261 ± 36 km s^{-1} (4)
179405	94384	9.12	B5	19500±2000	4.01±0.15	231±20	B2 V	–	–	
180126	94596	7.99	B3p	20000±1500	3.80±0.10	243±20	B2 IV	–	–	
181231	94988	8.58	B9V	14000±1000	3.73±0.10	250±30	B5 IV	–	–	
181308	-01°3711	8.70	B8	14000±1000	3.78±0.10	246±15	B5 IV	1.02±0.15	0.23±0.09	
181367	+02°3852	9.36	B8	13500±1000	3.65±0.15	279±30	B6 IV	0.55±0.08	0.05±0.07	
181709	95133	8.79	B8	13500±1000	3.24±0.20	249±10	B6 III	0.60±0.09	0.05±0.07	
181803	95152	9.1	B9	12000±500	3.±0.25	185±50	B7 III	–	–	

ID		SIMBAD		This work						
HD/BD	HIP/BD/ MWC	V	Sp. Type	$T_{\rm eff}$ (K)	log g (c.g.s.)	V sin i (km s^{-1})	Sp. Type	$W_{\lambda}^{H\gamma}$ (mÅ)	r	Notes
184279	96196	6.98	B0.5IV	28000±2000	4.00±0.20	230±30	B0 V	–	–	$T_{\rm eff}$ =30400 ± 600 K (5) log g = 3.9 ± 0.1 (5) Vsin i = 200 ± 22 km s^{-1} (5) Vsin i = 212 ± 9 km s^{-1} (4) $T_{\rm eff}$ = 30408 K (6) log g = 3.92 (6) Vsin i = 195 ± 20 (6)
184767	96403	7.179	A2	10000±500	3.52±0.10	44±15	A0 III	0.15±0.02	–	
194244	100664	6.144	B9V	10500±500	3.31±0.08	233±15	B9 III	0.25±0.04	–	Vsin i = 222 km s^{-1} (1) Vsin i = 175 km s^{-1} (3) Vsin i = 221 ± 14 km s^{-1} (4) Vsin i = 220 km s^{-1} (14)
230579	+10°3774	9.10	B1.5:IV:ne	29500±1500	3.85±0.15	330±40	B1 IV	0.45±0.07	–	
-09°4858	MWC964	8.84	B	21000±1500	4.10±0.20	108±20	B1.5 V	1.33±0.20	0.35±0.11	

Table 5. Fundamental parameters corrected for the effects of fast rotation at different Ω/Ω_c ratios. Error bars on the parameters are of the same order than in Table 4. When the projected rotation velocity was greater than the break-up speed or than the equatorial speed, the cells were left blank.

	$\Omega/\Omega_c = 0.80$				$\Omega/\Omega_c = 0.90$				$\Omega/\Omega_c = 0.95$				$\Omega/\Omega_c = 0.99$			
HD	T^{o}_{eff} (K)	$\log g_o$ (cgs)	$V\sin i_{true}$ (km s^{-1})	i (°)	T^{o}_{eff} (K)	$\log g_o$ (cgs)	$V\sin i_{true}$ (km s^{-1})	i (°)	T^{o}_{eff} (K)	$\log g_o$ (cgs)	$V\sin i_{true}$ (km s^{-1})	i (°)	T^{o}_{eff} (K)	$\log g_o$ (cgs)	$V\sin i_{true}$ (km s^{-1})	i (°)
42406									16500	3.96	338	61	17000	3.97	360	79
43264													12000	3.16	284	79
43285	15000	4.03	266	71	15000	3.99	274	55	15000	3.95	292	51	15000	3.93	309	58
44783	12000	3.37	226	93	12000	3.40	227	80	11500	3.13	231	82	11500	3.21	218	57
45901	27000	3.78	171	31	27000	3.79	173	26	27500	3.84	175	24	29500	4.06	174	21
46380	23500	3.91	306	65	23500	3.92	310	49	23500	3.94	315	44	23500	3.96	325	41
46484	27500	3.69	127	25	26500	3.61	130	21	29000	3.81	128	19	28000	3.69	134	15
47054	13000	3.60	220	78	13000	3.58	229	59	13000	3.51	239	54	12500	3.47	253	51
47160	11500	3.76	150	39	11500	3.74	158	33	11500	3.69	161	35	11500	3.70	173	33
47359									32500	4.03	469	73	32000	4.01	486	71
49330	26500	3.87	280	59	26500	3.86	285	46	28500	3.96	285	37	27000	3.87	296	34
49567	17500	3.58	93	26	17500	3.58	94	21	18000	3.61	99	20	18000	3.62	99	18
49585	26500	4.03	318	73	26000	4.10	325	57	25000	4.20	332	50	27500	4.09	331	41
49787	25500	4.09	167	29	25500	4.09	169	24	25500	4.10	172	22	25500	4.13	175	18
50083	21000	3.58	188	45	21000	3.61	193	37	21000	3.64	196	33	21500	3.68	199	30
50138	12500	3.27	67	21	12500	3.27	69	18	12500	3.27	66	16	12500	3.23	73	15
50209	13000	3.66	202	89	13000	3.64	209	64	13000	3.57	219	57	12500	3.53	230	55
50581	11000	3.77	236	79	11000	3.65	250	78	11000	3.66	251	64	10500	3.64	250	54
50696					24000	3.85	366	78	25000	3.88	366	61	23500	3.75	375	49
50868	23500	4.43	273	49	23500	4.47	276	39	23500	4.46	278	35	24000	4.52	284	31
50891	28500	4.00	227	45	28000	4.02	231	37	29000	4.05	233	32	29000	4.08	239	29
51193	24000	3.73	221	46	24000	3.72	224	37	24000	3.74	228	34	24000	3.79	233	31
51404	24500	4.45	347	68	24000	4.45	353	52	24500	4.49	358	47	25000	4.53	363	41
51452	31000	4.02	306	59	30500	3.99	309	46	31500	4.04	313	41	30500	3.99	325	39
51506	18000	3.98	183	37	18000	4.01	186	31	18000	3.99	195	29	18000	3.98	204	28
52721					24000	4.26	364	65	24500	4.29	368	51	24500	4.33	377	45
53085	16000	3.90	212	54	16000	3.88	222	45	16000	3.86	231	42	11500	3.80	247	40
53667	29000	3.56	116	23	27500	3.46	119	19	30000	3.66	118	17	31000	3.77	118	14
54464	17500	3.55	172	51	18000	3.55	177	42	18000	3.57	182	40	18000	3.56	191	38
55135	18000	4.56	254	55	18000	4.55	264	55	18000	4.55	273	44	18000	4.52	290	39
55606	26500	4.32	357	65	27000	4.34	361	49	28500	4.45	364	44	28000	4.43	377	41
55806																
57539	14500	3.42	149	46	14000	3.40	155	39	14000	3.37	159	36	14000	3.32	171	34
166917	12500	3.36	170	58	12500	3.35	173	46	12500	3.29	169	46	12500	3.28	184	44
168797	20000	3.69	271	79	20500	3.75	279	55	21000	3.71	288	48	21000	3.74	302	45
170009	11500	3.56	182	68	11500	3.45	181	53	11500	3.43	193	49	11000	3.44	204	47
170714	24500	4.06	277	53	24500	4.07	280	44	24500	4.06	283	38	24500	4.10	290	35
171219					16000	3.53	314	85	15500	3.53	314	83	16500	3.70	339	77
173219	27500	3.73	63	11	27500	3.74	66	9	29000	3.92	65	9	29500	3.96	66	8
173371	13500	3.88	278	92	13500	3.83	295	78	13500	3.77	313	69	13500	3.79	312	73
173530	13500	3.43	239	94	13500	3.45	246	80	14000	3.51	249	80	13500	3.33	277	71
173637	26500	3.64	207	43	28000	3.79	207	35	28000	3.78	208	29	29000	3.93	213	29
173817	14000	3.94	267	76	14000	3.90	276	57	14000	3.85	296	55	14000	3.84	317	59
174513	24000	3.95	256	57	24000	3.96	261	49	24000	3.98	264	43	24000	4.02	270	38
174571	22000	4.14	246	51	22000	4.20	250	42	22500	4.25	252	36	23000	4.31	259	30
174705					23500	4.10	341	69	23500	4.10	346	58	24000	4.15	357	51
174886	15000	3.49	77	21	15000	3.50	79	18	15000	3.49	79	17	15000	3.47	83	16
175869	12500	3.52	168	58	12000	3.47	171	47	12000	3.40	180	44	12000	3.39	196	43
176159	14500	3.92	236	74	14500	3.89	243	62	14500	3.89	258	58	14500	3.80	270	58
176630	17000	3.40	185	56	17000	3.41	188	45	17000	3.40	197	42	17000	3.37	211	40
178479	17000	4.06	106	24	17000	4.08	109	20	17000	4.07	116	19	17000	4.07	117	18
179343	11500	3.09	148	55	12000	3.07	155	45	11500	3.02	158	43	11500	2.98	167	40
179405	20000	4.19	237	44	20500	4.23	248	36	21000	4.27	247	32	21000	4.30	258	30
180126	21000	3.98	250	60	21500	4.02	252	48	21500	4.09	259	42	21500	4.08	267	39
181231	14500	3.96	257	66	14500	3.90	259	52	14500	3.93	275	54	14500	3.83	295	54

Table 5. Continued ...

	$\Omega/\Omega_c = 0.80$				$\Omega/\Omega_c = 0.90$				$\Omega/\Omega_c = 0.95$				$\Omega/\Omega_c = 0.99$			
HD	T^{o}_{eff} (K)	$\log g_o$ (cgs)	$V\sin i_{true}$ (km s^{-1})	i (°)	T^{o}_{eff} (K)	$\log g_o$ (cgs)	$V\sin i_{true}$ (km s^{-1})	i (°)	T^{o}_{eff} (K)	$\log g_o$ (cgs)	$V\sin i_{true}$ (km s^{-1})	i (°)	T^{o}_{eff} (K)	$\log g_o$ (cgs)	$V\sin i_{true}$ (km s^{-1})	i (°)
181308	15000	4.00	254	64	15000	3.97	261	51	15000	3.93	277	48	15000	3.91	293	52
181367	14500	3.94	282	78	14500	3.88	292	62	14500	3.86	308	56	14500	3.76	331	56
181709													14500	3.40	291	90
181803					13000	3.19	190	79	12500	3.08	186	66	12500	3.11	210	62
184279	30500	4.05	135	22	31000	4.08	137	19	31000	4.10	140	17	31000	4.08	145	16
184767	10000	3.51	49	16	10500	3.55	49	13	10000	3.43	46	13	10000	3.53	50	10
194244	11500	3.59	234	84	11000	3.52	232	79	11000	3.40	256	70	11000	3.42	247	61
230579	31000	4.03	338	72	30000	3.92	343	47	32000	4.07	346	47	31500	4.08	352	38
BD-09°4858	21500	4.18	115	22	22000	4.22	115	17	22000	4.27	117	15	22000	4.31	117	14

Table 7: List of *pnrc* surface-*averaged* parameters and their respective interpolated masses $M/M_{\odot}$, ages τ, and fractional ages $\tau/\tau_{\rm MS}$. When the projected rotation velocity was greater than the break-up speed or than the equatorial speed, the Table were left blank. Can be downloaded from the CDS.

HD	$T_{\rm eff}^{\rm surf.}$	log $g^{\rm surf.}$	log $L/L_{\odot}$ $^{\rm surf.}$	M/M$_{\odot}$	age (years)	$\tau/\tau_{\rm MS}$
$\Omega/\Omega_{\rm c}$ = 0.80						
42406						
43264						
43285	14500±1100	4.02±0.17	2.69± 0.09	4.60± 0.30	0.665E+08±0.201E+08	0.47± 0.13
44783	11500±1100	3.33±0.21	2.94± 0.12	4.30± 0.30	0.166E+09±0.155E+08	1.02± 0.03
45901	26000±2300	3.74±0.21	4.43± 0.13	13.60± 1.30	0.122E+08±0.200E+07	0.75± 0.10
46380	23000±1100	3.88±0.14	3.94± 0.12	10.00± 0.60	0.166E+08±0.256E+07	0.62± 0.09
46484	27000±1000	3.64±0.13	4.65± 0.14	15.70± 1.30	0.110E+08±0.604E+06	0.80± 0.04
47054	12500± 800	3.58±0.15	2.87± 0.12	4.60± 0.20	0.132E+09±0.110E+08	0.91± 0.05
47160	11500± 600	3.74±0.11	2.41± 0.08	3.60± 0.10	0.208E+09±0.169E+08	0.79± 0.05
47359						
49330	26000±1700	3.84±0.17	4.30± 0.12	12.80± 1.00	0.118E+08±0.195E+07	0.69± 0.10
49567	17000±1700	3.56±0.22	3.58± 0.12	7.00± 0.60	0.477E+08±0.646E+07	0.91± 0.07
49585	26000±1700	4.00±0.16	4.11± 0.09	12.00± 0.90	0.876E+07±0.265E+07	0.45± 0.12
49787	25000±1200	4.07±0.12	3.93± 0.08	10.90± 0.60	0.796E+07±0.250E+07	0.34± 0.10
50083	20500±1100	3.56±0.15	4.04± 0.12	9.60± 0.60	0.255E+08±0.191E+07	0.89± 0.04
50138	12500±1100	3.23±0.19	3.22± 0.13	5.10± 0.40	0.113E+09±0.100E+08	1.02± 0.02
50209	12750±1700	3.63±0.28	2.82± 0.14	4.50± 0.40	0.133E+09±0.262E+08	0.87± 0.11
50581	10500± 600	3.74±0.11	2.26± 0.07	3.30± 0.10	0.260E+09±0.227E+08	0.78± 0.05
50696						
50868	22500±1600	4.42±0.15	3.29± 0.07	8.10± 0.20		
50891	27500±2300	3.97±0.22	4.29± 0.16	13.60± 1.50	0.816E+07±0.239E+07	0.49± 0.14
51193	23000±1200	3.70±0.12	4.19± 0.09	11.10± 0.50	0.173E+08±0.131E+07	0.79± 0.05
51404	23500±1900	4.44±0.14	3.37± 0.10	8.70± 0.80		
51452	30000±1700	3.99±0.16	4.51± 0.12	16.40± 1.40	0.571E+07±0.162E+07	0.43± 0.12
51506	17500±1100	3.96±0.17	3.17± 0.12	6.10± 0.40	0.393E+08±0.948E+07	0.55± 0.12
52721						
53085	15500± 800	3.87±0.12	2.99± 0.08	5.30± 0.20	0.658E+08±0.891E+07	0.66± 0.07
53667	28000±1700	3.51±0.14	4.96± 0.09	19.30± 1.40	0.898E+07±0.566E+06	0.87± 0.03
54464	17000±1700	3.52±0.22	3.67± 0.13	7.30± 0.60	0.440E+08±0.545E+07	0.92± 0.06
55135	17618±1100	4.27±0.21	2.84±0.20	5.64±0.46	0.134E+08±0.660E+07	0.16±0.08
55606	26000±2300	4.30±0.21	3.76± 0.13	10.80± 1.30	0.180E+06±0.293E+07	0.01± 0.14
55806						
57539	14000±1100	3.39±0.18	3.31± 0.10	5.50± 0.40	0.907E+08±0.802E+07	1.00± 0.03
166917	12000±1100	3.32±0.20	3.08± 0.12	4.70± 0.30	0.136E+09±0.119E+08	1.02± 0.03
168797	19500±1100	3.66±0.15	3.78± 0.12	8.20± 0.50	0.319E+08±0.283E+07	0.82± 0.06
170009	11500± 600	3.54±0.17	2.65± 0.16	4.00± 0.20	0.192E+09±0.156E+08	0.93± 0.05
170714	24000±1400	4.04±0.16	3.86± 0.12	10.20± 0.70	0.104E+08±0.327E+07	0.39± 0.12
171219						
173219	26500±2300	3.69±0.22	4.56± 0.18	14.80± 1.70	0.116E+08±0.168E+07	0.79± 0.10
173371	13000± 600	3.86±0.11	2.58± 0.08	4.10± 0.20	0.127E+09±0.130E+08	0.67± 0.06
173530	13000±1100	3.40±0.19	3.16± 0.10	5.10± 0.30	0.111E+09±0.106E+08	1.00± 0.03
173637	25500±1700	3.60±0.15	4.57± 0.10	14.40± 1.00	0.128E+08±0.101E+07	0.85± 0.05
173817	14000±1100	3.92±0.19	2.67± 0.12	4.40± 0.30	0.953E+08±0.229E+08	0.61± 0.12
174513	23500±1700	3.92±0.17	3.95± 0.10	10.30± 0.80	0.146E+08±0.356E+07	0.57± 0.12
174571	21000±1700	4.12±0.19	3.47± 0.10	8.10± 0.60	0.108E+08±0.602E+07	0.26± 0.13
174705						
174886	14500± 600	3.47±0.10	3.32± 0.08	5.80± 0.20	0.796E+08±0.432E+07	0.97± 0.02
175869	12000± 600	3.49±0.11	2.86± 0.08	4.40± 0.20	0.151E+09±0.992E+07	0.96± 0.03
176159	14500±1100	3.90±0.18	2.76± 0.10	4.60± 0.30	0.868E+08±0.184E+08	0.63± 0.11
176630	16500±1100	3.36±0.17	3.74± 0.13	7.20± 0.60	0.491E+08±0.429E+07	1.00± 0.03
178479	16500±1100	4.04±0.16	2.94± 0.08	5.50± 0.30	0.399E+08±0.131E+08	0.43± 0.12

179343	11500±1100	3.05±0.22	3.27± 0.18	5.20± 0.50	0.106E+09±0.126E+08	1.02± 0.00
179405	19500±2300	4.17±0.27	3.19±0.16	6.87±0.77	0.186E+08±0.705E+07	0.28±0.10
180126	20000±1700	3.96±0.19	3.53± 0.10	7.80± 0.60	0.230E+08±0.672E+07	0.53± 0.13
181231	14000±1100	3.94±0.18	2.71± 0.10	4.60± 0.30	0.844E+08±0.210E+08	0.58± 0.12
181308	14500±1100	3.98±0.17	2.74± 0.10	4.70± 0.30	0.697E+08±0.197E+08	0.52± 0.13
181367	14500±1100	3.92±0.18	2.75±0.12	4.67±0.30	0.802E+08±0.136E+08	0.57±0.08
181709						
181803						
184279	30000±2300	4.02±0.22	4.45± 0.17	15.90± 1.80	0.540E+07±0.203E+07	0.39± 0.14
184767	10000± 600	3.49±0.13	2.39± 0.08	3.40± 0.20	0.309E+09±0.285E+08	0.97± 0.03
194244	11000± 600	3.57±0.11	2.54± 0.07	3.80± 0.10	0.217E+09±0.151E+08	0.91± 0.04
230579	30000±1700	4.00±0.16	4.49±0.12	16.33±1.36	0.544E+07±0.116E+07	0.40±0.08
BD-09º4858	21000±1700	4.16±0.21	3.37± 0.15	7.60± 0.70	0.884E+07±0.636E+07	0.19± 0.13
$\Omega/\Omega_c = 0.90$						
42406						
43264						
43285	14500±1100	3.95±0.18	2.70± 0.10	4.60± 0.30	0.819E+08±0.201E+08	0.57± 0.12
44783	11500±1100	3.35±0.20	2.94± 0.12	4.40± 0.30	0.161E+09±0.151E+08	1.02± 0.03
45901	26000±2200	3.74±0.21	4.42± 0.13	13.50± 1.30	0.125E+08±0.196E+07	0.75± 0.10
46380	22500±1100	3.87±0.14	3.91± 0.12	9.80± 0.60	0.177E+08±0.264E+07	0.64± 0.09
46484	25500±1000	3.54±0.13	4.65± 0.14	15.10± 1.30	0.124E+08±0.606E+06	0.87± 0.03
47054	12500± 800	3.54±0.16	2.89± 0.12	4.60± 0.20	0.133E+09±0.117E+08	0.93± 0.05
47160	11000± 600	3.69±0.11	2.44± 0.07	3.70± 0.10	0.211E+09±0.154E+08	0.83± 0.05
47359						
49330	25500±1700	3.80±0.17	4.30± 0.12	12.60± 1.00	0.127E+08±0.190E+07	0.74± 0.09
49567	17000±1700	3.54±0.22	3.57± 0.12	7.00± 0.50	0.488E+08±0.638E+07	0.92± 0.06
49585	25000±1700	4.05±0.16	3.95± 0.09	11.00± 0.80	0.847E+07±0.317E+07	0.37± 0.12
49787	24500±1100	4.04±0.12	3.92± 0.08	10.70± 0.60	0.936E+07±0.257E+07	0.39± 0.10
50083	20500±1100	3.55±0.15	4.02± 0.12	9.40± 0.60	0.253E+08±0.189E+07	0.86± 0.04
50138	12000±1200	3.21±0.19	3.21± 0.13	5.10± 0.40	0.113E+09±0.988E+07	1.02± 0.02
50209	12500±1700	3.60±0.28	2.83± 0.14	4.50± 0.40	0.135E+09±0.250E+08	0.90± 0.10
50581	10500± 600	3.61±0.12	2.37± 0.07	3.50± 0.10	0.263E+09±0.200E+08	0.89± 0.04
50696	23500±1700	3.80±0.18	4.06± 0.12	10.60± 0.80	0.169E+08±0.273E+07	0.70± 0.09
50868	22500±1100	4.43±0.39	3.24± 0.43	7.90± 1.10		
50891	27000±2200	3.97±0.22	4.25± 0.16	13.20± 1.40	0.839E+07±0.263E+07	0.49± 0.14
51193	23000±1100	3.66±0.12	4.19± 0.09	11.10± 0.50	0.180E+08±0.126E+07	0.81± 0.04
51404	23500±1900	4.42±0.15	3.35± 0.09	8.50± 0.70		
51452	29500±1700	3.94±0.16	4.50± 0.12	15.80± 1.30	0.714E+07±0.170E+07	0.52± 0.14
51506	17000±1100	3.97±0.17	3.13± 0.12	6.00± 0.40	0.402E+08±0.101E+08	0.54± 0.12
52721	23500±2200	4.23±0.27	3.57± 0.22	9.10± 1.00	0.262E+07±0.465E+07	0.08± 0.14
53085	15500± 800	3.83±0.12	3.00± 0.08	5.30± 0.20	0.707E+08±0.839E+07	0.70± 0.07
53667	26500±1700	3.38±0.14	4.97± 0.09	18.90± 1.40	0.972E+07±0.561E+06	0.92± 0.03
54464	17000±1700	3.50±0.22	3.67± 0.13	7.40± 0.60	0.443E+08±0.606E+07	0.93± 0.06
55135	17500±1100	4.25±0.21	2.83±0.20	5.59±0.45	0.156E+08±0.707E+07	0.18±0.08
55606	26000±2200	4.31±0.21	3.77± 0.14	10.90± 1.30	0.136E+06±0.274E+07	0.01± 0.14
55806	13000±1100	3.58±0.19	2.90± 0.10	4.70± 0.30	0.125E+09±0.150E+08	0.91± 0.06
57539	13500±1100	3.34±0.18	3.31± 0.10	5.50± 0.40	0.938E+08±0.767E+07	1.01± 0.03
166917	12000±1100	3.29±0.20	3.07± 0.13	4.70± 0.30	0.137E+09±0.117E+08	1.02± 0.03
168797	19500±1100	3.70±0.15	3.76± 0.12	8.30± 0.50	0.304E+08±0.289E+07	0.80± 0.06
170009	11000± 600	3.40±0.17	2.71± 0.16	3.90± 0.20	0.215E+09±0.151E+08	1.00± 0.03
170714	23500±1400	4.03±0.16	3.82± 0.12	9.90± 0.70	0.115E+08±0.347E+07	0.42± 0.12
171219	15500± 800	3.48±0.14	3.42± 0.12	6.20± 0.30	0.658E+08±0.471E+07	0.96± 0.03
173219	26500±2200	3.68±0.22	4.55± 0.18	14.60± 1.70	0.119E+08±0.170E+07	0.79± 0.10
173371	13000± 600	3.79±0.10	2.70± 0.08	4.40± 0.20	0.122E+09±0.978E+07	0.75± 0.05
173530	13000±1100	3.40±0.18	3.15± 0.10	5.10± 0.30	0.111E+09±0.104E+08	1.00± 0.03
173637	27000±1700	3.73±0.15	4.53± 0.09	14.70± 1.00	0.111E+08±0.119E+07	0.75± 0.06
173817	13500±1100	3.85±0.19	2.68± 0.12	4.40± 0.30	0.109E+09±0.213E+08	0.68± 0.11

174513	23000±1700	3.92±0.17	3.91± 0.10	10.00± 0.80	0.156E+08±0.368E+07	0.58± 0.12
174571	21000±1700	4.16±0.19	3.42± 0.10	8.00± 0.60	0.835E+07±0.584E+07	0.20± 0.12
174705	22500±1700	4.06±0.18	3.68± 0.10	9.10± 0.70	0.122E+08±0.479E+07	0.38± 0.13
174886	14500± 600	3.46±0.10	3.30± 0.08	5.70± 0.20	0.816E+08±0.441E+07	0.97± 0.02
175869	12000± 600	3.43±0.12	2.86± 0.08	4.30± 0.20	0.164E+09±0.117E+08	0.99± 0.02
176159	14000±1100	3.85±0.18	2.76± 0.10	4.60± 0.30	0.973E+08±0.181E+08	0.68± 0.10
176630	16000±1100	3.35±0.17	3.71± 0.13	7.10± 0.50	0.509E+08±0.430E+07	1.00± 0.03
178479	16500±1100	4.04±0.16	2.91± 0.09	5.40± 0.30	0.418E+08±0.132E+08	0.43± 0.12
179343	11500±1100	3.01±0.21	3.30± 0.18	5.30± 0.60	0.996E+08±0.126E+08	1.02± 0.00
179405	19500±2200	4.19±0.27	3.18±0.16	6.92±0.77	0.172E+08±0.665E+07	0.27±0.10
180126	20500±1700	3.97±0.19	3.54± 0.10	7.90± 0.60	0.214E+08±0.646E+07	0.51± 0.13
181231	13500±1100	3.86±0.18	2.72± 0.10	4.50± 0.30	0.102E+09±0.195E+08	0.68± 0.10
181308	14500±1100	3.93±0.17	2.74± 0.10	4.70± 0.30	0.818E+08±0.190E+08	0.59± 0.12
181367	14000±1100	3.84±0.18	2.77±0.12	4.64±0.29	0.943E+08±0.1261E+08	0.66±0.07
181709						
181803	12500± 600	3.13±0.19	3.36± 0.22	5.50± 0.70	0.914E+08±0.134E+08	1.02± 0.01
184279	30000±2300	4.03±0.22	4.44± 0.18	15.80± 1.80	0.534E+07±0.204E+07	0.38± 0.14
184767	10000± 600	3.51±0.13	2.37± 0.08	3.40± 0.10	0.304E+09±0.220E+08	0.96± 0.03
194244	10500± 600	3.48±0.12	2.58± 0.07	3.80± 0.20	0.231E+09±0.192E+08	0.97± 0.03
230579	28500±1700	3.87±0.16	4.53±0.12	15.76±1.29	0.804E+07±0.106E+07	0.58±0.07
BD-09º4858	21000±1700	4.18±0.23	3.36± 0.19	7.70± 0.70	0.651E+07±0.595E+07	0.14± 0.13
$\Omega/\Omega_c = 0.99$						
42406	16000±1100	3.91±0.16	3.01± 0.09	5.50± 0.30	0.574E+08±0.114E+08	0.62± 0.10
43264	11500± 600	3.08±0.11	3.21± 0.09	5.10± 0.30	0.112E+09±0.739E+07	1.02± 0.00
43285	14000±1100	3.87±0.17	2.77± 0.10	4.70± 0.30	0.919E+08±0.173E+08	0.67± 0.10
44783	11000±1100	3.13±0.21	3.04± 0.14	4.60± 0.30	0.143E+09±0.128E+08	1.02± 0.01
45901	28000±2200	3.98±0.20	4.34± 0.12	14.30± 1.40	0.733E+07±0.233E+07	0.47± 0.14
46380	22500±1100	3.89±0.14	3.87± 0.12	9.60± 0.60	0.177E+08±0.273E+07	0.62± 0.09
46484	26500±1000	3.60±0.13	4.66± 0.14	15.70± 1.30	0.113E+08±0.580E+06	0.83± 0.04
47054	12000± 800	3.40±0.16	2.92± 0.12	4.40± 0.30	0.155E+09±0.133E+08	1.00± 0.03
47160	11000± 600	3.63±0.12	2.45± 0.08	3.60± 0.10	0.226E+09±0.177E+08	0.88± 0.04
47359	30500±2200	3.93±0.19	4.63± 0.13	17.70± 1.80	0.625E+07±0.166E+07	0.52± 0.13
49330	26000±1700	3.79±0.17	4.33± 0.12	13.00± 1.00	0.123E+08±0.176E+07	0.71± 0.09
49567	17000±1700	3.54±0.22	3.60± 0.12	7.10± 0.60	0.463E+08±0.595E+07	0.92± 0.06
49585	26000±1700	4.02±0.16	4.10± 0.09	12.10± 0.90	0.813E+07±0.256E+07	0.43± 0.13
49787	24500±1100	4.06±0.12	3.87± 0.08	10.40± 0.60	0.928E+07±0.274E+07	0.37± 0.10
50083	20500±1100	3.59±0.14	4.00± 0.12	9.40± 0.60	0.247E+08±0.190E+07	0.84± 0.04
50138	12000±1100	3.15±0.19	3.26± 0.13	5.20± 0.40	0.104E+09±0.894E+07	1.02± 0.01
50209	12000±1700	3.46±0.29	2.88± 0.15	4.40± 0.40	0.152E+09±0.233E+08	0.98± 0.07
50581	10000± 600	3.58±0.12	2.26± 0.07	3.20± 0.10	0.320E+09±0.288E+08	0.91± 0.04
50696	22500±1700	3.67±0.18	4.12± 0.12	10.60± 0.80	0.196E+08±0.229E+07	0.80± 0.07
50868	22500±1100	4.46±0.33	3.22± 0.36	8.00± 1.00		
50891	27500±2200	4.00±0.23	4.26± 0.18	13.60± 1.50	0.731E+07±0.256E+07	0.44± 0.15
51193	23000±1100	3.71±0.12	4.14± 0.09	10.90± 0.50	0.178E+08±0.146E+07	0.77± 0.05
51404	23500±1700	4.47±0.16	3.31± 0.07	8.50± 0.60		
51452	29000±1700	3.91±0.16	4.51± 0.13	15.80± 1.30	0.762E+07±0.161E+07	0.56± 0.11
51506	17000±1100	3.91±0.16	3.18± 0.12	6.10± 0.40	0.435E+08±0.870E+07	0.61± 0.11
52721	23000±2200	4.27±0.23	3.50± 0.14	8.80± 1.00	0.123E+07±0.436E+07	0.03± 0.14
53085	15000± 800	3.73±0.12	3.05± 0.08	5.30± 0.20	0.793E+08±0.698E+07	0.80± 0.05
53667	29500±1700	3.69±0.13	4.85± 0.09	18.90± 1.30	0.819E+07±0.712E+06	0.76± 0.05
54464	17000±1700	3.49±0.22	3.68± 0.13	7.40± 0.60	0.442E+08±0.585E+07	0.94± 0.06
55135	17000±1100	4.22±0.22	2.82±0.21	5.53±0.46	0.185E+08±0.767E+07	0.21±0.09
55606	26500±1300	4.37±0.23	3.74±0.14	11.0±0.50		
55806	12500±1100	3.43±0.19	2.95± 0.10	4.60± 0.30	0.141E+09±0.143E+08	0.99± 0.04
57539	13500±1100	3.24±0.17	3.38± 0.10	5.70± 0.30	0.865E+08±0.635E+07	1.02± 0.01
166917	11500±1100	3.20±0.20	3.12± 0.13	4.80± 0.30	0.127E+09±0.110E+08	1.02± 0.01
168797	20000±1100	3.67±0.15	3.81± 0.12	8.50± 0.50	0.294E+08±0.255E+07	0.82± 0.06

170009	10500± 600	3.37±0.17	2.68± 0.16	3.80± 0.30	0.228E+09±0.208E+08	1.01± 0.03
170714	23500±1300	4.03±0.16	3.81± 0.12	9.80± 0.70	0.117E+08±0.350E+07	0.42± 0.12
171219	15500± 800	3.62±0.14	3.30± 0.12	6.00± 0.30	0.644E+08±0.500E+07	0.88± 0.05
173219	28000±2200	3.88±0.21	4.45± 0.16	14.80± 1.60	0.892E+07±0.211E+07	0.60± 0.13
173371	12500± 600	3.72±0.10	2.69± 0.08	4.30± 0.20	0.138E+09±0.943E+07	0.81± 0.04
173530	12500±1100	3.25±0.18	3.23± 0.10	5.20± 0.30	0.108E+09±0.808E+07	1.02± 0.02
173637	28000±1700	3.85±0.15	4.45± 0.09	14.60± 1.10	0.958E+07±0.154E+07	0.64± 0.09
173817	13500±1100	3.78±0.19	2.74± 0.12	4.50± 0.30	0.116E+09±0.177E+08	0.76± 0.09
174513	23000±1700	3.95±0.17	3.86± 0.10	9.80± 0.80	0.151E+08±0.401E+07	0.54± 0.13
174571	21500±1700	4.25±0.24	3.36± 0.21	8.00± 0.90	0.249E+07±0.456E+07	0.06± 0.14
174705	22500±1700	4.08±0.17	3.67± 0.09	9.10± 0.70	0.108E+08±0.459E+07	0.34± 0.13
174886	14500± 600	3.40±0.10	3.34± 0.08	5.70± 0.30	0.829E+08±0.517E+07	1.00± 0.02
175869	11500± 600	3.31±0.11	2.91± 0.09	4.30± 0.20	0.170E+09±0.102E+08	1.02± 0.01
176159	13500±1100	3.73±0.18	2.84± 0.10	4.70± 0.30	0.109E+09±0.151E+08	0.80± 0.08
176630	16000±1100	3.29±0.16	3.76± 0.13	7.30± 0.50	0.492E+08±0.368E+07	1.02± 0.02
178479	16500±1100	4.00±0.16	2.94± 0.09	5.50± 0.30	0.466E+08±0.131E+08	0.50± 0.12
179343	11000±1100	2.90±0.22	3.34± 0.18	5.50± 0.60	0.925E+08±0.125E+08	1.02± 0.00
179405	20000±2200	4.25±0.27	3.15±0.16	6.99±0.76	0.134E+08±0.588E+07	0.21±0.09
180126	20500±1700	4.01±0.19	3.48± 0.10	7.80± 0.60	0.197E+08±0.670E+07	0.45± 0.13
181231	13500±1100	3.76±0.18	2.79± 0.10	4.60± 0.30	0.110E+09±0.162E+08	0.77± 0.08
181308	14000±1100	3.84±0.17	2.81± 0.10	4.70± 0.30	0.914E+08±0.160E+08	0.70± 0.10
181367	15000±1100	3.76±0.17	2.99±0.12	5.21±0.32	0.795E+08±0.808E+07	0.75±0.06
181709	13500±1100	3.32±0.20	3.31± 0.17	5.50± 0.50	0.942E+08±0.927E+07	1.02± 0.03
181803	12000± 600	3.03±0.18	3.38± 0.22	5.60± 0.80	0.875E+08±0.143E+08	1.02± 0.00
184279	29500±2200	4.00±0.22	4.43± 0.18	15.50± 1.80	0.610E+07±0.209E+07	0.43± 0.14
184767	9500± 600	3.46±0.13	2.37± 0.08	3.30± 0.20	0.323E+09±0.266E+08	0.98± 0.03
194244	10000± 600	3.35±0.12	2.62± 0.07	3.70± 0.10	0.259E+09±0.150E+08	1.02± 0.02
230579	30000±1700	4.00±0.16	4.49±0.13	16.40±1.33	0.535E+07±0.114E+07	0.43±0.09
BD-09°4858	21000±1700	4.25±0.19	3.29± 0.12	7.60± 0.70	0.258E+07±0.480E+07	0.06± 0.11